RAPIDLY SHEARED COMPRESSIBLE TURBULENCE: CHARACTERIZATION OF DIFFERENT PRESSURE REGIMES AND EFFECT OF THERMODYNAMIC FLUCTUATIONS

A Thesis

by

REBECCA LYNNE BERTSCH

Submitted to the Office of Graduate Studies of
Texas A&M University
in partial fulfillment of the requirements for the degree of

MASTER OF SCIENCE

August 2010

Major Subject: Aerospace Engineering

RAPIDLY SHEARED COMPRESSIBLE TURBULENCE: CHARACTERIZATION OF DIFFERENT PRESSURE REGIMES AND EFFECT OF THERMODYNAMIC FLUCTUATIONS

A Thesis

by

REBECCA LYNNE BERTSCH

Submitted to the Office of Graduate Studies of
Texas A&M University
in partial fulfillment of the requirements for the degree of

MASTER OF SCIENCE

Approved by:

Chair of Committee,	Sharath Girimaji
Committee Members,	Jacques Richard
	Prabir Daripa
Head of Department,	Dimitris Lagoudas

August 2010

Major Subject: Aerospace Engineering

ABSTRACT

Rapidly Sheared Compressible Turbulence:
Characterization of Different Pressure Regimes and Effect of Thermodynamic Fluctuations. (August 2010)
Rebecca Lynne Bertsch, B.A., Colorado College
Chair of Advisory Committee: Dr. Sharath Girimaji

Rapid distortion theory (RDT) is applied to compressible ideal-gas turbulence subjected to homogeneous shear flow. The study examines the linear or rapid processes present in turbulence evolution. Specific areas of investigation include:(i) characterization of the multi-stage flow behavior,(ii) changing role of pressure in the three-regime evolution and (iii) influence of thermodynamic fluctuations on the different regimes. Preliminary investigations utilizing the more accurate Favre-averaged RDT approach show promise however, this approach requires careful validation and testing.

In this study the Favre-averaged RDT approach is validated against Direct Numerical Simulation (DNS) and Reynolds-averaged RDT results. The three-stage growth of the flow field statistics is first confirmed. The three regime evolution of turbulence is then examined in three different timescales and the physics associated with each regime is discussed in depth. The changing role of pressure in compressible turbulence evolution shows three distinct stages. The physics of each stage is clearly explained. Next, the influence of initial velocity and thermodynamic fluctuations on the flow field are investigated. The evolution of turbulence is shown to be strongly dependent on the initial gradient Mach number and initial temperature fluctuations which tend to delay the onset of the second regime of evolution. The initial turbulent Mach number, which quantifies velocity fluctuations in the flow, influences turbulence evolution only weakly. Comparison of Reynolds-averaged RDT against

Favre-averaged RDT for simulations of nonzero initial flow field fluctuations shows the higher fidelity of the latter approach.

To my family who have always urged me to do my best.

ACKNOWLEDGMENTS

I would like to take this opportunity to thank everyone who aided me during my graduate career and helped me complete my Master's thesis. First of all, I would like to thank my graduate advisor, Dr. Sharath Girimaji, for helping me develop the necessary research skills to be successful. His unique teaching ability has aided me in understanding the fundamental concepts of fluid turbulence. I would like to thank Dr. Jacques Richard and Dr. Prabir Daripa for their participation on my committee and giving relevant feedback in the thesis writing process. My research with Dr. Richard in summer 2006 was my first experience in turbulence and was a major influence on my graduate career. The coursework I took with Dr. Daripa was invaluable to my research. I would like to thank the staff of the Aerospace Engineering Department for all their help. Special thanks to Karen Knabe for her expertise in the Thesis/Dissertation paperwork deadlines.

I would like to personally thank Sawan Suman for acting as a mentor throughout my graduate career. Sawan's knowledge of my field of research greatly influenced my understanding of my work . Even after completion of his dissertation he continued to respond to my inquisitive emails and verify my research results. I also appreciate the support and assistance the rest of my research group has given me in the past three years. Our weekly turbulence discussions have given me insight into other areas of research.

I must acknowledge my family and friends back home in Colorado who continue to support me even though they wish I weren't so far away.

And finally, to all my amazing friends in the department, thanks for your support, discussions and laughter.

This work was supported by NASA MURI research grant and the Hypersonics

Center at Texas A & M University.

TABLE OF CONTENTS

CHAPTER Page

LIST OF TABLES

LIST OF FIGURES

FIGURE Page

FIGURE Page

FIGURE Page

CHAPTER I

INTRODUCTION

A century and a half after the development of the Navier-Stokes equations, the phenomenon of fluid turbulence continues to confound scientists and engineers alike. Turbulence is a multiscale chaotic phenomenon comprised of several competing elementary processes. Even with several of these processes and their complex interactions only partially understood, researchers have uncovered ways to model turbulent flows adequately for many applications. Yet much needs to be done to improve our understanding of the basic physics of turbulence and enhance the capabilities of predictive engineering tools.

A. Motivation

Over the last few decades, computers have played an increasingly influential role in turbulence research. There exist several different approaches of varying degrees of complexity to compute or simulate turbulence (Figure 1). The most accurate of these approaches, Direct Numerical Simulation(DNS), computes all scales of motion. As a result DNS requires excessive computational power, as the computational effort increases as the cube of the Reynolds number. Another approach, commonly known as Large Eddy Simulation, directly resolves the large spatial scales which are flow dependent, and models the small scales which are considered to be universal. Both of these approaches are high in accuracy, but they are impractical for realistic applications since they are limited to smaller Reynolds numbers. At the present time, the statistical Reynolds-Averaged Navier-Stokes (RANS) method offers the best avenue

---

The journal model is *IEEE Transactions on Automatic Control.*

for computing practical flows.

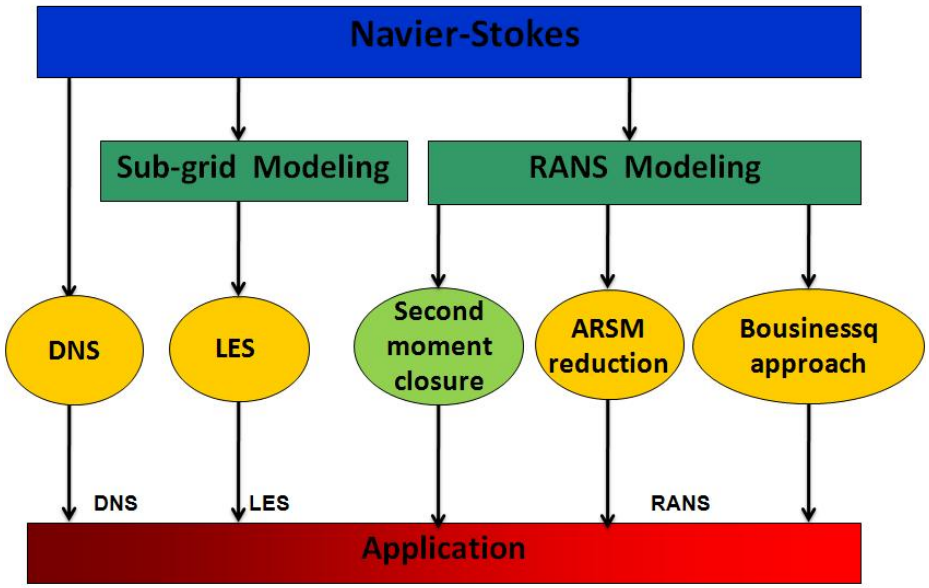

Fig. 1. Schematic of various approaches for turbulence calculations. Decreasing order of accuracy and computational effort from left to right.

Several (RANS) approaches of varying degrees of sophistication have been developed over the last several decades. These methods require only a small fraction of the computational power of previously mentioned approaches. The RANS equations by themselves are unclosed due to the appearance of statistical moments, so the turbulence-model equations are used to close the set of equations. RANS models can be broadly classified into three categories, which in order of increasing closure modeling accuracy are: (i)Bousinesq approach, (ii) Algebraic Reynolds Stress Model(ARSM), and (iii) Second moment closure model (SMC). In the first two approaches, an algebraic constitutive relationship between Reynolds stress and mean velocity gradient tensor is sought. In the SMC approach, evolution equations are solved for the Reynolds stresses. Several terms in the Reynolds-Stress evolution equations

(RSEE) require closure modeling. These terms include: (i) pressure-strain correlation (ii) dissipation, and (iii) turbulent transport (see Figure 2). Compressible flow turbulence encompasses further complexities as a result of interactions between flow and thermodynamic variables. Closure modeling of the SMC level can ultimately increase the fidelity of lower order models as shown in Figure 2. Using the weak equilibrium assumption a 2-eqn ARSM can be derived from SMC. Further, using the averaging invariance principle, a hybrid (Partially-Averaged Navier-Stokes) model can be derived. Therefore, closure modeling at the SMC level has several important benefits.

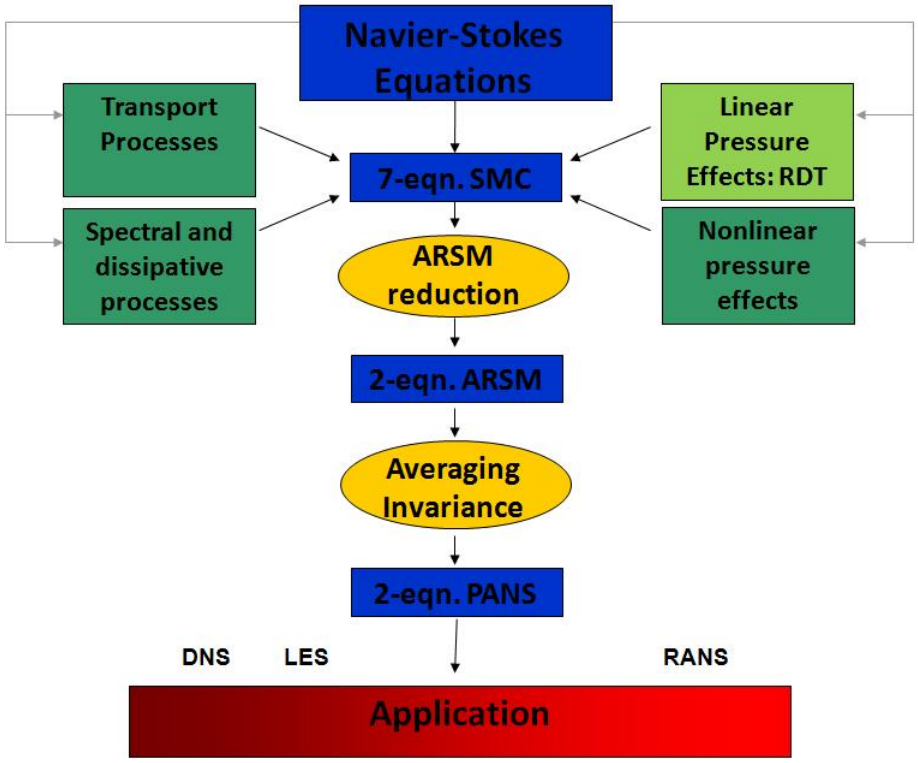

Fig. 2. Roadmap of steps required to apply different approaches to realistic scenarios. RDT provides second moment closure modeling to obtain the 7-equation SMC.

B. Rapid Distortion Theory: A Literature Review

One of the most important terms requiring closure modeling at the SMC level in incompressible and compressible flows is the rapid pressure-strain correlation [1]. The linear rapid distortion theory (RDT), first introduced in the mid-1950s [2], governs the behavior of rapid pressure strain correlation. Figure 2 shows how RDT can improve closure modeling at all RANS levels including hybrid methods such as Partially-Averaged Navier-Stokes (PANS). Previous examinations of incompressible RDT have led to a greater understanding of the rapid pressure-strain redistribution process leading to improved closure modeling of RANS based approaches: e.g. flows with system rotation [3, 4] and axial compression through a pipe [2]. At the present time, incompressible RDT is considered to be an approach that is well developed and the underlying physics is reasonably well understood. Studies on compressible RDT have been more recent. By examining linearized compressible Navier-Stokes equations we can investigate the changing role of the rapid pressure-strain correlation term in different Mach number regimes. Most compressible RDT studies to date employ the isentropic flow conditions [3, 5, 6, 7, 8, 9].

More recent work related to this study [10, 11, 12, 13] employs more realistic thermodynamic treatments. Livescu and Madnia [14] were the first to use an equation of state, but their work was restricted to examining decoupled flow statistics only. The next step was taken by Yu and Girimaji [10] who developed the equations for RDT of ideal-gas compressible turbulence and performed preliminary investigations of thermodynamic statistics. Lavin [13] further investigated the coupling between flow and thermodynamic fields in rapidly distorted homogeneous shear compressible turbulence. While tangible progress has been made over the last few years in understanding compressibility effects in rapidly sheared flows, many questions still remain

and a complete picture is yet to emerge.

C. Research Goals

To address crucial questions that still remain, the objective of this study is twofold: (1) to characterize and demarcate the various stages of pressure behavior as a function of Mach number, (2) examine the effect of thermodynamic fluctuations on various regimes of pressure behavior.

The procedure for this study is as follows. We use two RDT approaches (Reynolds-averaged and Favre-averaged) to investigate turbulence behavior in various timescales of interest. These timescales are:(i) Shear time, (ii) acoustic time and (iii) mixed time. Next we demonstrate the different physical features of the various regimes of turbulence evolution. From this we determine the role that pressure plays within each regime. We establish the ranges of the different regimes in terms of elapsed time and the gradient Mach number. Finally, we examine how the various regimes of pressure behavior are influenced by (i) initial temperature fluctuation intensity, T_s and (ii) initial turbulent Mach number, M_t . These investigations expand upon previous studies of compressible RDT and yield an improved understanding of the physics associated with compressible homogeneous shear flow.

D. Thesis Outline

The remainder of the thesis is arranged as follows. In Chapter II, we present the Reynolds and Favre-averaged RDT equations. Validation of the methodology against DNS data is also given. In Chapter III we demonstrate the need for multiple timescales and present an in depth examination of the three-stage behavior of compressible rapidly sheared flows. Chapter IV provides final validation of the improved capabili-

ties of the Favre-averaged equations through examination of the polytropic coefficient. We present further studies on the influence of thermodynamic fluctuations on flow field behavior in Chapter V. We end the thesis by summarizing the key conclusions and discuss the direction of future work in this field.

CHAPTER II

RAPID DISTORTION THEORY FOR COMPRESSIBLE FLOWS

A. Reynolds Averaged Statistics

First, we outline the development of the Reynolds-averaged RDT equations and discuss the assumptions and the range of parameters investigated.

1. Methodology

The development of the inviscid R-RDT equations for ideal-gas compressible flow was first presented in [10]. The equations that govern this type of flow field are the inviscid conservation equations for compressible flow and the state equation for an ideal gas.

$$\frac{\partial \rho}{\partial t} + U_j \frac{\partial \rho}{\partial x_j} = -\rho \frac{\partial U_j}{\partial x_j} \tag{2.1}$$

$$\frac{\partial U_i}{\partial t} + U_j \frac{\partial U_i}{\partial x_j} = -\frac{1}{\rho} \frac{\partial P}{\partial x_i} \tag{2.2}$$

$$\frac{\partial T}{\partial t} + U_j \frac{\partial T}{\partial x_j} = -(\gamma - 1) T \frac{\partial U_j}{\partial x_j} \tag{2.3}$$

$$P = \rho R T \tag{2.4}$$

where γ is the ratio of specific heats, ρ is the density, U is the velocity, T is the temperature and P is pressure.

We decompose the instantaneous variables of density, velocity, temperature and pressure into their mean and fluctuating components using Reynolds decomposition: $\rho = \overline{\rho} + \rho'$, $U_i = \overline{U_i} + u_i{}'$, $T = \overline{T} + T'$ and $P = \overline{P} + P'$. This averaging method uses

unweighted means and the governing equations are now written as:

$$\frac{\partial(\overline{\rho}+\rho')}{\partial t}+(\overline{U_j}+u_j{}')\frac{\partial(\overline{\rho}+\rho')}{\partial x_j}=-(\overline{\rho}+\rho')\frac{\partial(\overline{U_j}+u_j{}')}{\partial x_j} \tag{2.5}$$

$$\frac{\partial(\overline{U_j}+u_j{}')}{\partial t}+(\overline{U_j}+u_j{}')\frac{\partial(\overline{U_i}+u_i{}')}{\partial x_j}=-\frac{1}{(\overline{\rho}+\rho')}\frac{\partial(\overline{P}+P')}{\partial x_i} \tag{2.6}$$

$$\frac{\partial(\overline{T}+T')}{\partial t}+(\overline{U_j}+u_j{}')\frac{\partial(\overline{T}+T')}{\partial x_j}=-(\gamma-1)(\overline{T}+T')\frac{\partial(\overline{U_j}+u_j{}')}{\partial x_j} \tag{2.7}$$

$$\overline{P}+P'=R\overline{\rho}\overline{T}+R\overline{\rho}T'+R\rho'\overline{T}+R\rho'T' \tag{2.8}$$

In order to find the mean equations we must first deal with the decomposed density in the denominator of Eq. (2.6) by using a Taylor expansion:

$$\frac{1}{(\overline{\rho}+\rho')}=\frac{1}{\overline{\rho}}-\frac{\rho'}{(\overline{\rho})^2}+\frac{(\rho')^2}{(\overline{\rho})^3}-... \tag{2.9}$$

After applying the series expansion and taking the mean of Equations 2.5-2.8 we are left with the averaged governing equations:

$$\frac{\partial\overline{\rho}}{\partial t}+\overline{U_j}\frac{\partial\overline{\rho}}{\partial x_j}=-\overline{\rho}\frac{\partial\overline{U_j}}{\partial x_j}-\frac{\partial\overline{\rho' u_j{}'}}{\partial x_j} \tag{2.10}$$

$$\frac{\partial\overline{U_j}}{\partial t}+\overline{U_j}\frac{\partial\overline{U_i}}{\partial x_j}+\overline{u_j{}'\frac{\partial u_i{}'}{\partial x_j}}=-\frac{1}{\overline{\rho}}\frac{\partial\overline{P}}{\partial x_i}+\frac{1}{(\overline{\rho})^2}\overline{\rho'\frac{\partial P'}{\partial x_i}}-\frac{\overline{(\rho')^2}}{(\overline{\rho})^3}\frac{\partial\overline{P}}{\partial x_i} \tag{2.11}$$

$$\frac{\partial\overline{T}}{\partial t}+\overline{U_j}\frac{\partial\overline{T}}{\partial x_j}+\overline{u_j{}'\frac{\partial T'}{\partial x_j}}=-(\gamma-1)\overline{T}\frac{\partial\overline{U_j}}{\partial x_j}-(\gamma-1)\overline{T'\frac{\partial u_j{}'}{\partial x_j}} \tag{2.12}$$

$$\overline{P}=R\overline{\rho}\overline{T}+R\overline{\rho'T'} \tag{2.13}$$

We neglect all terms that are third order or higher in fluctuations, just as in in-

compressible RDT. The previous set of Equations 2.10-2.13, make up the Reynolds averaged first-order statistics which are accurate to second order in fluctuations. To find the second-order statistics we must develop the set of equations further.

To find the fluctuating equations we simply subtract the mean set, Equations 2.10-2.13, from the instantaneous set, Equations 2.5-2.8. Subtracting Eq 2.10 from Eq. 2.5 gives the fluctuating mass conservation equation:

$$\begin{aligned}\frac{\partial \rho'}{\partial t} + \overline{U_k}\frac{\partial \rho'}{\partial x_k} = &- u_k{}'\frac{\partial \overline{\rho}}{\partial x_k} - u_k{}'\frac{\partial \rho'}{\partial x_k} + \overline{u_k{}'\frac{\partial \rho'}{\partial x_k}} - \overline{\rho}\frac{\partial u_k{}'}{\partial x_k} \\ &- \rho'\frac{\partial \overline{U_k}}{\partial x_k} - \rho'\frac{\partial u_k{}'}{\partial x_k} + \overline{\rho'\frac{\partial u_k{}'}{\partial x_k}}\end{aligned} \tag{2.14}$$

The fluctuating momentum equation, found by subtracting Eq. 2.11 from Eq. 2.6 is:

$$\begin{aligned}\frac{\partial u_i{}'}{\partial t} + \overline{U_k}\frac{\partial u_i{}'}{\partial x_k} = &- u_k{}'\frac{\partial \overline{U_i}}{\partial x_k} - u_k{}'\frac{\partial u_i{}'}{\partial x_k} + \overline{u_k{}'\frac{\partial u_i{}'}{\partial x_k}} - \frac{1}{\overline{\rho}}\frac{\partial P'}{\partial x_i} + \frac{\rho'}{(\overline{\rho})^2}\frac{\partial \overline{P}}{\partial x_i} \\ &+ \frac{\rho'}{(\overline{\rho})^2}\frac{\partial P'}{\partial x_i} - \frac{(\rho')^2}{(\overline{\rho})^3}\frac{\partial \overline{P}}{\partial x_i} - \frac{1}{(\overline{\rho})^2}\overline{\rho'\frac{\partial P'}{\partial x_i}} + \frac{\overline{(\rho')^2}}{(\overline{\rho})^3}\frac{\partial \overline{P}}{\partial x_i}\end{aligned} \tag{2.15}$$

We opt to develop the fluctuating pressure equation first. The fluctuating pressure equation can be found by subtracting Eq. 2.13 from Eq. 2.8 we are left with:

$$P' = R\overline{\rho}T' + R\rho'\overline{T} + R\rho'T' - R\overline{\rho'T'} \tag{2.16}$$

We substitute Eq. 2.16 into Eq. 2.15 to give:

$$\begin{aligned}\frac{\partial u_i'}{\partial t}+\overline{U_k}\frac{\partial u_i'}{\partial x_k}= &- u_k'\frac{\partial \overline{U_i}}{\partial x_k}-u_k'\frac{\partial u_i'}{\partial x_k}+\overline{u_k'\frac{\partial u_i'}{\partial x_k}}+\frac{\rho'}{(\overline{\rho})^2}\frac{\partial \overline{P}}{\partial x_i}\\ &- \frac{(\rho')^2}{(\overline{\rho})^3}\frac{\partial \overline{P}}{\partial x_i}+\overline{\frac{(\rho')^2}{(\overline{\rho})^3}\frac{\partial \overline{P}}{\partial x_i}}\\ &- \frac{R}{(\overline{\rho})^2}\overline{\rho'(\frac{\partial \overline{\rho}T'}{\partial x_i}+\frac{\partial \rho'\overline{T}}{\partial x_i})}\\ &- \frac{R}{\overline{\rho}}\frac{\partial}{\partial x_i}(\overline{\rho}T'+\rho'\overline{T}+\rho'T'-\overline{\rho'T'})\\ &+ \frac{R\rho'}{(\overline{\rho})^2}\frac{\partial}{\partial x_i}(\overline{\rho}T'+\rho'\overline{T})\end{aligned} \tag{2.17}$$

The last fluctuating equation is the energy equation found by subtracting Eq. 2.12 from Eq. 2.7:

$$\begin{aligned}\frac{\partial T'}{\partial t}+\overline{U_k}\frac{\partial T'}{\partial x_k}= &- u_k'\frac{\partial \overline{T}}{\partial x_k}-u_k'\frac{\partial T'}{\partial x_k}+\overline{u_k'\frac{\partial T'}{\partial x_k}}-(\gamma-1)\overline{T}\frac{\partial u_k'}{\partial x_k}\\ &- (\gamma-1)T'\frac{\partial \overline{U_k}}{\partial x_k}-(\gamma-1)T'\frac{\partial u_k'}{\partial x_k}+(\gamma-1)\overline{T'\frac{\partial u_k'}{\partial x_k}}\end{aligned} \tag{2.18}$$

Equations 2.14, 2.17 and 2.18 comprise the governing fluctuation equations. Next, we apply some important RDT assumptions to simplify our set of equations.

a. Homogeneity Assumption

Thus far the only assumption we have utilized is that third-order or higher fluctuation terms are negligible. The equations developed above govern inviscid compressible turbulence evolving according to the ideal gas law. From this point on we will assume a homogeneous flow field. By applying this assumption we can reduce the complexity of the above equations. The homogeneity condition forces the mean thermodynamic variables and mean velocity gradients to be uniform throughout the flow field:

$$\frac{\partial \overline{T}}{\partial x_i}=\frac{\partial \overline{P}}{\partial x_i}=\frac{\partial \overline{\rho}}{\partial x_i}=0 \tag{2.19}$$

$$\frac{\partial \overline{U_i}}{\partial x_j}(\overrightarrow{x}, t) = \frac{\partial \overline{U_i}}{\partial x_j}(t) \tag{2.20}$$

These homogeneity requirements are satisfied only in shear flows. For other types of mean flows, further analytical treatments are necessary and such flows are excluded from this study.

As a result, the moments of the thermodynamic and velocity fluctuation variables become spatially independent:

$$\frac{\partial}{\partial x_i}\overline{\phi'\phi'} = \frac{\partial}{\partial x_i}\overline{\phi'\phi'\phi'} = ... = 0 \tag{2.21}$$

Applying the homogeneity condition to Equations 2.14, 2.17 and 2.18, we find the rapid distortion equations for the fluctuating fields to be:

$$\frac{d\rho'}{dt} = -\frac{\partial(u_k{}'\rho')}{\partial x_k} - \overline{\rho}\frac{\partial u_k{}'}{\partial x_k} - \rho'\frac{\partial \overline{U_k}}{\partial x_k} \tag{2.22}$$

$$\begin{aligned}\frac{du_i{}'}{dt} = & - u_k{}'\frac{\partial \overline{U_i}}{\partial x_k} - u_k{}'\frac{\partial u_i{}'}{\partial x_k} + \overline{u_k{}'\frac{\partial u_i{}'}{\partial x_k}} - \frac{RT'}{\overline{\rho}}\overline{\rho'\frac{\partial T'}{\partial x_i}} \\ & - R\frac{\partial T'}{\partial x_i} - \frac{R\overline{T}}{\overline{\rho}}\frac{\partial \rho'}{\partial x_i} - \frac{RT'}{\overline{\rho}}\frac{\partial \rho'}{\partial x_i} + \frac{R\overline{T}\rho'}{(\overline{\rho})^2}\frac{\partial \rho'}{\partial x_i}\end{aligned} \tag{2.23}$$

$$\begin{aligned}\frac{dT'}{dt} = & - u_k{}'\frac{\partial T'}{\partial x_k} + \overline{u_k{}'\frac{\partial T'}{\partial x_k}} - (\gamma-1)\overline{T}\frac{\partial u_k{}'}{\partial x_k} - (\gamma-1)T'\frac{\partial \overline{U_k}}{\partial x_k} \\ & - (\gamma-1)T'\frac{\partial u_k{}'}{\partial x_k} + (\gamma-1)\overline{T'\frac{\partial u_k{}'}{\partial x_k}}\end{aligned} \tag{2.24}$$

b. Linearization

Since RDT is a linear theory, the next step is to neglect all terms which are non-linear in fluctuations. Equations 2.22-2.24 become:

$$\frac{d\rho'}{dt} = -\overline{\rho}\frac{\partial u_k{}'}{\partial x_k} - \rho'\frac{\partial \overline{U_k}}{\partial x_k} \tag{2.25}$$

$$\frac{du_i'}{dt} = \quad - \quad u_k' \frac{\partial \overline{U_i}}{\partial x_k} - R\frac{\partial T'}{\partial x_i} - \frac{R\overline{T}}{\overline{\rho}}\frac{\partial \rho'}{\partial x_i} \tag{2.26}$$

$$\frac{dT'}{dt} = -(\gamma - 1)\overline{T}\frac{\partial u_k'}{\partial x_k} - (\gamma - 1)T'\frac{\partial \overline{U_k}}{\partial x_k} \tag{2.27}$$

c. Spectral Transformation

The linear RDT equations are solved in Fourier space to take advantage of the law of superposition. The Fourier transforms of the fluctuating terms are as follows:

$$\overrightarrow{u}'(\overrightarrow{x},t) = \sum \hat{\overrightarrow{u}}(t)e^{i\overrightarrow{\kappa}(t)\cdot\overrightarrow{x}}, \rho'(\overrightarrow{x},t) = \sum \hat{\rho}(t)e^{i\overrightarrow{\kappa}(t)\cdot\overrightarrow{x}}, T'(\overrightarrow{x},t) = \sum \hat{T}(t)e^{i\overrightarrow{\kappa}(t)\cdot\overrightarrow{x}} \tag{2.28}$$

where $\overrightarrow{\kappa}$ is the wavenumber vector and $\hat{\overrightarrow{u}}$, $\hat{\rho}$, and $\hat{T}$ are the Fourier coefficients of velocity, density and temperature fluctuations, respectively. Applying the Fourier transforms to Equations 2.37-39 turns the set of partial differential equations into a set of ordinary differential equations:

$$\frac{d\hat{\rho}}{dt} = -i\overline{\rho}\kappa_k\hat{u_k} - \hat{\rho}\frac{\partial \overline{U_k}}{\partial x_k} \tag{2.29}$$

$$\frac{d\hat{u_j}}{dt} = -\hat{u_k}\frac{\partial \overline{U_j}}{\partial x_k} - i(R\hat{T} + \frac{R\overline{T}}{\overline{\rho}}\hat{\rho})\kappa_j \tag{2.30}$$

$$\frac{dT'}{dt} = -i(\gamma - 1)\overline{T}\kappa_k\hat{u_k} - (\gamma - 1)\hat{T}\frac{\partial \overline{U_k}}{\partial x_k} \tag{2.31}$$

where $\imath$ is the imaginary unit number equal to $\sqrt{-1}$. To complete the set of ODEs, the wavenumber vector evolves as follows:

$$\frac{d\kappa_i}{dt} + \kappa_k\frac{\partial \overline{U_k}}{\partial x_i} = 0 \tag{2.32}$$

d. Particle Representation Method

From this point we may opt to directly solve Equations 2.41-44, and develop the covariances of the fluctuating terms. However, for this work we choose to follow the particle representation method presented in previous work by Kassinos and Reynolds [19]. Accordingly, we define the conditional moments based on wavenumbers as:

$$\hat{R}_{ij} \equiv \langle \hat{u}_i^* \hat{u}_j | \overrightarrow{\kappa} \rangle \tag{2.33}$$

$$\hat{L}_j \equiv \langle \hat{T}^* \hat{u}_j | \overrightarrow{\kappa} \rangle \tag{2.34}$$

$$\hat{M}_j \equiv \langle \hat{\rho}^* \hat{u}_j | \overrightarrow{\kappa} \rangle \tag{2.35}$$

$$\hat{A} \equiv \langle \hat{\rho}^* \hat{T} | \overrightarrow{\kappa} \rangle \tag{2.36}$$

$$\hat{B} \equiv \langle \hat{T}^* \hat{T} | \overrightarrow{\kappa} \rangle \tag{2.37}$$

$$\hat{C} \equiv \langle \hat{\rho}^* \hat{\rho} | \overrightarrow{\kappa} \rangle \tag{2.38}$$

Using Equations 2.41-2.43 we construct the evolution equations for the conditional moments of the fluctuating field:

$$\frac{d\hat{R}_{ij}}{dt} = -\frac{\partial \overline{U_i}}{\partial x_k}\hat{R}_{kj} - \frac{\partial \overline{U_j}}{\partial x_k}\hat{R}_{ik} + \imath R(\hat{L}_j\kappa_i - \hat{L}_i^*\kappa_j) + \imath\frac{R\overline{T}}{\overline{\rho}}(\hat{M}_j\kappa_i - \hat{M}_i^*\kappa_j) \tag{2.39}$$

$$\frac{d\hat{M}_i}{dt} = \imath\overline{\rho}\kappa_k\hat{R}_{ki} - \frac{\partial \overline{U_k}}{\partial x_k}\hat{M}_i - \frac{\partial \overline{U_i}}{\partial x_k}\hat{M}_k - \imath R\hat{A}\kappa_i - \imath\frac{R\overline{T}}{\overline{\rho}}\hat{C}\kappa_i \tag{2.40}$$

$$\frac{d\hat{L}_i}{dt} = \imath(\gamma-1)\overline{T}\kappa_k\hat{R}_{ki} - (\gamma-1)\frac{\partial \overline{U_k}}{\partial x_k}\hat{L}_i - \frac{\partial \overline{U_i}}{\partial x_k}\hat{L}_k - \imath R\hat{B}\kappa_i - \imath\frac{R\overline{T}}{\overline{\rho}}\hat{A}^*\kappa_o \tag{2.41}$$

$$\frac{d\hat{A}}{dt} = \imath\overline{\rho}\kappa_k\hat{L}_k^* - \imath(\gamma-1)\overline{T}\hat{M}_k\kappa_k - \gamma\frac{\partial \overline{U_k}}{\partial x_k}\hat{A} \tag{2.42}$$

$$\frac{d\hat{B}}{dt} = -2(\gamma-1)\frac{\partial \overline{U_k}}{\partial x_k}\hat{B} + \imath(\gamma-1)\overline{T}\kappa_k(\hat{L}_k^* - \hat{L}_k) \tag{2.43}$$

$$\frac{d\hat{C}}{dt} = -2\frac{\partial \overline{U_k}}{\partial x_k}\hat{C} + \imath\overline{\rho}\kappa_k(\hat{M}_k^* - \hat{M}_k) \tag{2.44}$$

We use equations 2.51-56 to solve for the conditional covariances. By summing over all the wavenumbers we obtain the second-order moments of the flucutations in physical-space:

$$\overline{u_i u_j} = \sum \hat{R}_{ij}(\overrightarrow{\kappa}, t) \tag{2.45}$$

$$\overline{u_i T} = \sum \hat{L}_i(\overrightarrow{\kappa}, t) \tag{2.46}$$

$$\overline{\rho u_i} = \sum \hat{M}_i(\overrightarrow{\kappa}, t) \tag{2.47}$$

$$\overline{\rho T} = \sum \hat{A}(\overrightarrow{\kappa}, t) \tag{2.48}$$

$$\overline{T^2} = \sum \hat{B}(\overrightarrow{\kappa}, t) \tag{2.49}$$

$$\overline{\rho^2} = \sum \hat{C}(\overrightarrow{\kappa}, t) \tag{2.50}$$

There are two advantages to following this approach of summing over all the wavenumbers: (i) it shows the clear correlation between several fluctuating moments and (ii)solving over all wave numbers increases the accuracy and computational efficiency. Since each of the covariances consist of real and imagimaginary components, we end up with a set of 26 ordinary differential equations that are solved simultaneously. To step in time we utilize a fourth-order Runge-Kutta scheme.

B. Favre-Averaged Statistics

Here we present the development of the Favre-averaged RDT equations in a format similar to that of Reynolds-averaged RDT.

1. Methodology

The pathway to derive the Favre-averaged fields is tangent to the approach outlined in the previous section. Once again, we begin with the inviscid conservation equations for compressible flow and the state equation for an ideal gas in a slightly different format:

$$\frac{\partial \rho}{\partial t} + \frac{\partial (\rho U_i)}{\partial x_i} = 0 \tag{2.51}$$

$$\frac{\partial (\rho U_i)}{\partial t} + \frac{\partial (\rho U_i U_j)}{\partial x_j} = -\frac{\partial P}{\partial x_i} \tag{2.52}$$

$$\frac{\partial (\rho T)}{\partial t} + \frac{\partial (\rho T U_j)}{\partial x_j} = -\frac{P}{c_v}\frac{\partial U_j}{\partial x_j} \tag{2.53}$$

$$P = \rho R T \tag{2.54}$$

where γ is the ratio of specific heats. The equations that govern the instantaneous flow field are the same as Reynolds-averaged RDT but when decomposing the field, we now utilize density weighted-mean components for velocity and temperature as shown below:

$$U_i = \frac{\overline{\rho U_i}}{\overline{\rho}} + u_i'' = \tilde{U}_i + u_i'' \tag{2.55}$$

$$T = \frac{\overline{\rho T}}{\overline{\rho}} + T'' = \tilde{T} + T'' \tag{2.56}$$

Reynolds decomposition is still applied to pressure and density variables. When applying the decomposition to the governing equations for the instantaneous flow field become:

$$\frac{\partial \rho}{\partial t} + \frac{\partial}{\partial x_i}\rho(\tilde{U}_i + {u_i}'') = 0 \tag{2.57}$$

$$\frac{\partial}{\partial t}\rho(\tilde{U}_i + {u_i}'') + \frac{\partial}{\partial x_j}(\rho(\tilde{U}_i + {u_i}'')(\tilde{U}_j + {u_j}'')) = -R\frac{\partial}{\partial x_i}\rho(\tilde{T} + T'') \tag{2.58}$$

$$\frac{\partial}{\partial t}\rho(\tilde{T} + T'') + \frac{\partial}{\partial x_j}\rho(\tilde{T} + T'')(\tilde{U}_j + {u_j}'') = -\frac{R\rho(\tilde{T} + T'')}{c_v}\frac{\partial(\tilde{U}_j + {u_j}'')}{\partial x_j} \tag{2.59}$$

$$P = \rho R(\tilde{T} + T'') \tag{2.60}$$

Notice we have already substituted the ideal gas equation into the momentum and energy equations. Taking the mean of these equations we find the conservation equations for the mean flow:

$$\frac{\partial \overline{\rho}}{\partial t} + \frac{\partial \overline{\rho}\tilde{U}_i}{\partial x_i} = -\frac{\partial \overline{\rho' {u_i}''}}{\partial x_i} \tag{2.61}$$

$$\frac{\partial(\overline{\rho}\tilde{U}_i)}{\partial t} + \frac{\partial}{\partial x_j}(\overline{\rho}\tilde{U}_i\tilde{U}_j + \overline{\rho {u_i}'' {u_j}''}) = -R\frac{\partial(\overline{\rho}\tilde{T})}{\partial x_i} \tag{2.62}$$

$$\begin{aligned} \frac{\partial(\overline{\rho}\tilde{T})}{\partial t} &+ \frac{\partial}{\partial x_j}(\overline{\rho}\tilde{T}\tilde{U}_j + \overline{\rho T'' {u_j}''}) \\ &= -\frac{R}{c_v}(\overline{\rho}\tilde{T}\frac{\partial \tilde{U}_j}{\partial x_j} + \tilde{T}\overline{\rho'\frac{\partial {u_j}''}{\partial x_j}} + \overline{\rho T''\frac{\partial {u_j}''}{\partial x_j}} + \overline{\rho T''\frac{\partial {u_j}''}{\partial x_j}}) \end{aligned} \tag{2.63}$$

As shown in Reynolds-averaged RDT development, the governing fluctuation equations are derived by subtracting the mean conservation equations from the in-

stantaneous flow field equations. Subtracting Equation 2.61 from Equation 2.57, the fluctuating mass equation is:

$$\frac{\partial \rho'}{\partial t} + \tilde{U}_j \frac{\partial \rho'}{\partial x_j} = -\frac{\partial (\rho u_i{}'')}{\partial x_i} - \rho' \frac{\partial \tilde{U}_i}{\partial x_i} \tag{2.64}$$

The fluctuating momentum equation, found by subtracting Equation 2.62 from Equation 2.58 is:

$$\begin{aligned} \frac{\partial (\rho u_i{}'')}{\partial t} + \tilde{U}_j \frac{\partial (\rho u_i{}'')}{\partial x_j} = & - \rho u_i{}'' \frac{\partial \tilde{U}_j}{\partial x_j} - \frac{\partial (\rho' \tilde{U}_i)}{\partial t} \\ & + \frac{\partial}{\partial x_j} (\overline{\rho u_i{}'' u_j{}''} - \rho' \tilde{U}_i \tilde{U}_j - \overline{\rho} \tilde{U}_i u_j{}'' - \overline{\rho} u_i{}'' u_j{}'' \\ & - \rho' \tilde{U}_i u_j{}'' - \rho' u_i{}'' u_j{}'') \\ & - R \frac{\partial}{\partial x_i} (\overline{\rho} T'' + \rho' \tilde{T} + \rho' T'') \end{aligned} \tag{2.65}$$

We have already substituted the ideal gas equation into our momentum equation in a previous step so it need not be done again. Instead, we now develop a second momentum equation which solves for the first order velocity fluctuations:

$$\begin{aligned} \rho (\frac{\partial u_i{}''}{\partial t} + \tilde{U}_j \frac{\partial u_i{}''}{\partial x_j}) = & - u_i{}'' (\frac{\partial \rho}{\partial t} + \tilde{U}_j \frac{\partial \rho}{\partial x_j}) - \rho u_i{}'' \frac{\partial \tilde{U}_j}{\partial x_j} \\ & - \rho' (\frac{\partial \tilde{U}_i}{\partial t} + \tilde{U}_j \frac{\partial \tilde{U}_i}{\partial x_j}) - \rho u_j{}'' \frac{\partial \tilde{U}_i}{\partial x_j} \\ & - \rho \frac{\partial}{\partial x_j} (u_i{}'' u_j{}'') - R \frac{\partial}{\partial x_i} (\rho T'') \\ & - R \rho'' \frac{\partial \tilde{T}}{\partial x_i} - R \tilde{T} \frac{\partial \rho'}{\partial x_i} \end{aligned} \tag{2.66}$$

Finally we find the fluctuating energy equation by subtracting equation 2.63 from

Equation 6.59:

$$\begin{aligned}\frac{\partial(\rho T'')}{\partial t}+\tilde{U}_j\frac{\partial(\rho T'')}{\partial x_j} = & - (\rho T'')\frac{\partial \tilde{U}_j}{\partial x_j}-\frac{\partial(\rho'\tilde{T})}{\partial t} \\ & - \frac{\partial}{\partial x_j}(\rho'\tilde{T}\tilde{U}_j+\rho\tilde{T}u_j{}''+\overline{\rho}u_j{}''T''-\overline{\rho u_i{}'' u_j{}''}) \\ & - \frac{R}{c_v}(\rho'\tilde{T}\frac{\partial \tilde{U}_j}{\partial x_j}+\rho\tilde{T}\frac{\partial u_j{}''}{\partial x_j}+\rho T''\frac{\partial \tilde{U}_j}{\partial x_j}+\rho T''\frac{\partial u_j{}''}{\partial x_j} \\ & - \tilde{T}\overline{\rho'\frac{\partial u_j{}''}{\partial x_j}}-\overline{\rho T''\frac{\partial u_j{}''}{\partial x_j}}-\overline{\rho T''\frac{\partial u_j{}''}{\partial x_j}}) \end{aligned} \tag{2.67}$$

Equations 2.64-67 comprise the governing fluctuating equations for Favre-averaged flow fields. Next, we continue to follow the Reynolds-averaged approach and apply the important RDT assumptions to simplify this set of equations.

a. Homogeneity Assumption

Once again the homogeneity condition forces the mean thermodynamic variables and the mean velociy gradient to be uniform in space:

$$\frac{\partial \tilde{T}}{\partial x_i}=\frac{\partial \overline{P}}{\partial x_i}=\frac{\partial \overline{\rho}}{\partial x_i}=0 \tag{2.68}$$

$$\frac{\partial \tilde{U}_j}{\partial x_j}(\overrightarrow{x},t)=\frac{\partial \tilde{U}_j}{\partial x_j}(t) \tag{2.69}$$

Again, only in shear flows are the homogeneity requirements satisfied. The moments of the thermodynamic and velocity fluctuation variables become spatially independent:

$$\frac{\partial}{\partial x_i}\overline{\phi'\phi'}=\frac{\partial}{\partial x_i}\overline{\phi'\phi'\phi'}=...=0 \tag{2.70}$$

Applying the homogeneity condition to Equations 2.64-67, we find the rapid distortion equations for the Favre-averaged fluctuating fields to be:

$$\frac{\partial \rho'}{\partial t}+\tilde{U}_j\frac{\partial \rho'}{\partial x_j}=-\frac{\partial(\rho u_i{}'')}{\partial x_i} \tag{2.71}$$

$$\frac{\partial(\rho u_i{}'')}{\partial t}+\tilde{U}_j\frac{\partial(\rho u_i{}'')}{\partial x_j}= - \tilde{U}_i(\frac{\partial\rho'}{\partial t}+\tilde{U}_j\frac{\partial\rho'}{\partial x_j})-\rho'(\frac{\partial\tilde{U}_i}{\partial t}+\tilde{U}_j\frac{\partial\tilde{U}_i}{\partial x_j}) - \rho\tilde{U}_i\frac{\partial u_j{}''}{\partial x_j}-\rho u_j{}''\frac{\partial\tilde{U}_i}{\partial x_j}-\tilde{U}_i u_j{}''\frac{\partial\rho'}{\partial x_j}-\rho\frac{\partial}{\partial x_j}(u_i{}''u_j{}'') - u_i{}''u_j{}''\frac{\partial\rho'}{\partial x_j}-R\overline{\rho}\frac{\partial T''}{\partial x_i}-R\tilde{T}\frac{\partial\rho'}{\partial x_i}-R\frac{\partial}{\partial x_i}(\rho'T'') \quad (2.72)$$

$$\rho(\frac{\partial u_i{}''}{\partial t}+\tilde{U}_j\frac{\partial u_i{}''}{\partial x_j})= - u_i{}''(\frac{\partial\rho}{\partial t}+\tilde{U}_j\frac{\partial\rho}{\partial x_j})-\rho'(\frac{\partial\tilde{U}_i}{\partial t} + \tilde{U}_j\frac{\partial\tilde{U}_i}{\partial x_j})-\rho u_j{}''\frac{\partial\tilde{U}_i}{\partial x_j}-\rho\frac{\partial}{\partial x_j}(u_i{}''u_j{}'') - R\frac{\partial}{\partial x_i}(\rho T'')-R\rho{}''\frac{\partial\tilde{T}}{\partial x_i} - R\tilde{T}\frac{\partial\rho'}{\partial x_i} \quad (2.73)$$

$$\frac{\partial(\rho T'')}{\partial t}+\tilde{U}_j\frac{\partial(\rho T'')}{\partial x_j}= - (\frac{\partial(\rho'\tilde{T})}{\partial t}+\tilde{U}_j\frac{\partial(\rho'\tilde{T})}{\partial x_j})-\rho\tilde{T}\frac{\partial u_j{}''}{\partial x_j} - \tilde{T}u_j{}''\frac{\partial\rho'}{\partial x_j}-\overline{\rho}u_j{}''\frac{\partial T''}{\partial x_j}-\overline{\rho}T''\frac{\partial u_j{}''}{\partial x_j} - \frac{R}{c_v}(\rho\tilde{T}\frac{\partial u_j{}''}{\partial x_j}+\rho T''\frac{\partial u_j{}''}{\partial x_j}-\tilde{T}\overline{\rho'\frac{\partial u_j{}''}{\partial x_j}} - \overline{\rho T''\frac{\partial u_j{}''}{\partial x_j}}-\overline{\rho T''}\frac{\partial u_j{}''}{\partial x_j}) \quad (2.74)$$

b. Linearization

Since RDT is a linear theory, the next step is to neglect all terms which are non-linear in fluctuations. The linearized Favre-averaged fluctuating equations are:

$$\frac{d\rho'}{dt}=-\frac{\partial(\rho u_i{}'')}{\partial x_i} \quad (2.75)$$

$$\frac{d(\rho u_i{}'')}{dt}=-\rho u_j{}''\frac{\partial\tilde{U}_i}{\partial x_j}-R\frac{\partial(\rho T'')}{\partial x_i}-R\tilde{T}\frac{\partial\rho'}{\partial x_i} \quad (2.76)$$

$$\frac{d(u_i{}'')}{dt} = -u_j{}''\frac{\partial \tilde{U}_i}{\partial x_j} - \frac{R}{\overline{\rho}}\frac{\partial(\rho T'')}{\partial x_i} - \frac{R\tilde{T}}{\overline{\rho}}\frac{\partial \rho'}{\partial x_i} \tag{2.77}$$

$$\frac{d(\rho T'')}{dt} = -\rho u_j{}''\frac{\partial \tilde{T}}{\partial x_j} - \frac{R\overline{\rho}\tilde{T}}{c_v}\frac{\partial u_j{}''}{\partial x_j} \tag{2.78}$$

c. Spectral Transformation

Continuing along the same path as R-RDT development, we transforming the fluctuating quantities to Fourier space in order to turn the above PDEs into ODEs:

$$\frac{d\hat{\rho}'}{dt} = -\imath\kappa_m\hat{\alpha}_m \tag{2.79}$$

$$\frac{d\hat{u}_i''}{dt} = -\hat{u}_m''\frac{\partial \tilde{U}_i}{\partial x_m} - \imath\kappa_i\frac{R}{\overline{\rho}}(\hat{\beta} + \tilde{T}\hat{\rho}') \tag{2.80}$$

$$\frac{d\hat{\alpha}_i}{dt} = -\hat{\alpha}_m\frac{\partial \tilde{U}_i}{\partial x_m} - \imath R\kappa_i(\hat{\beta} + \tilde{T}\rho') \tag{2.81}$$

$$\frac{d\hat{\beta}}{dt} = -\imath(\gamma-1)\overline{\rho}\tilde{T}\kappa_m\hat{u_m}'' \tag{2.82}$$

where the new Greek letters represent:

$$\alpha_i = \rho u_i{}'' \tag{2.83}$$

$$\beta = \rho T'' \tag{2.84}$$

Again, we close the set of ODE's with the evolution of the wavenumber vector:

$$\frac{d\kappa_i}{dt} + \kappa_k\frac{\partial \overline{U_k}}{\partial x_i} = 0 \tag{2.85}$$

d. Particle Representation Method

For Favre-averaged fields, the conditional moments based upon wavenumber are:

$$\hat{A}_{ij} = \langle \hat{u_i^*}\hat{u_j}|\overrightarrow{\kappa}\rangle \tag{2.86}$$

$$\hat{B}_{ij} = \langle \hat{\alpha_i^*} \hat{\alpha_j} | \overrightarrow{\kappa} \rangle \tag{2.87}$$

$$\hat{C}_{ij} = \langle \hat{\alpha_i^*} \hat{u_j} | \overrightarrow{\kappa} \rangle \tag{2.88}$$

$$\hat{D}_i = \langle \hat{u_i^*} \hat{\rho} | \overrightarrow{\kappa} \rangle \tag{2.89}$$

$$\hat{E}_i = \langle \hat{\alpha_i^*} \hat{\rho} | \overrightarrow{\kappa} \rangle \tag{2.90}$$

$$\hat{F}_i = \langle \hat{u_i^*} \hat{\beta} | \overrightarrow{\kappa} \rangle \tag{2.91}$$

$$\hat{G}_i = \langle \hat{\alpha_i^*} \hat{\beta} | \overrightarrow{\kappa} \rangle \tag{2.92}$$

$$\hat{H} = \langle \hat{\beta}^* \hat{\rho} | \overrightarrow{\kappa} \rangle \tag{2.93}$$

$$\hat{I} = \langle \hat{\rho}^* \hat{\rho} | \overrightarrow{\kappa} \rangle \tag{2.94}$$

$$\hat{J} = \langle \hat{\beta}^* \hat{\beta} | \overrightarrow{\kappa} \rangle \tag{2.95}$$

The final step in development of Favre-averaged RDT is to construct the evolution equations of the conditional moments using Equations 2.79-82. After doing so we substitute in the appropriate labels above (Equations 2.86-95) and the fluctuating moments for Favre-averaged fields are:

$$\frac{dA_{ij}}{dt} = -A_{mj}\frac{\partial \tilde{U}_i}{\partial x_m} - A_{im}\frac{\partial \tilde{U}_i}{\partial x_m} + \imath\kappa_i \frac{R}{\overline{\rho}}(F_j^* + \tilde{T}D_j^*) - \imath\kappa_i \frac{R}{\overline{\rho}}(F_i + \tilde{T}D_i) \tag{2.96}$$

$$\frac{dB_{ij}}{dt} = -B_{mj}\frac{\partial \tilde{U}_i}{\partial x_m} - B_{im}\frac{\partial \tilde{U}_j}{\partial x_m} + \imath R\kappa_i(G_j^* + \tilde{T}E_j^*) - \imath R\kappa_j(G_i + \tilde{T}E_i) \tag{2.97}$$

$$\frac{dC_{ij}}{dt} = -C_{mj}\frac{\partial \tilde{U}_i}{\partial x_m} - C_{im}\frac{\partial \tilde{U}_j}{\partial x_m} + \imath R\kappa_i(F_j^* + \tilde{T}D_j^*) - \imath\kappa_j \frac{R}{\overline{\rho}}(G_i + \tilde{T}E_i) \tag{2.98}$$

$$\frac{dD_i}{dt} = -D_m\frac{\partial \tilde{U}_i}{\partial x_m} + \imath\kappa_i \frac{R}{\overline{\rho}}(H + \tilde{T}I) - \imath\kappa_m C_{mi}^* \tag{2.99}$$

$$\frac{dE_i}{dt} = -E_m\frac{\partial \tilde{U}_i}{\partial x_m} + \imath R\kappa_i(H + \tilde{T}I) - \imath\kappa_m B_{im} \tag{2.100}$$

$$\frac{dF_i}{dt} = -F_m\frac{\partial \tilde{U}_i}{\partial x_m} + \imath\kappa_i \frac{R}{\overline{\rho}}(J + \tilde{T}H^*) - \imath(\gamma - 1)\overline{\rho}\tilde{T}\kappa_m A_{im} \tag{2.101}$$

$$\frac{dG_i}{dt} = -G_m \frac{\partial \tilde{U}_i}{\partial x_m} + \imath R \kappa_i (J + \tilde{T} H^*) - \imath(\gamma - 1)\overline{\rho}\tilde{T}\kappa_m C_{im} \tag{2.102}$$

$$\frac{dH}{dt} = \imath \kappa_m [(\gamma - 1)\overline{\rho}\tilde{T} D_m - G_m^*] \tag{2.103}$$

$$\frac{dI}{dt} = \imath \kappa_m (E_m - E_m^*) \tag{2.104}$$

$$\frac{dJ}{dt} = \imath(\gamma - 1)\overline{\rho}\tilde{T}\kappa_m (F_m - F_m^*) \tag{2.105}$$

Once again, by summing over all wavenumbers we obtain the second and third order moments of the fluctuating field in physical space:

$$\overline{u_i u_j} = \sum_{\overrightarrow{\kappa}} \hat{A}_{ij}(\overrightarrow{\kappa}, t) \tag{2.106}$$

$$\overline{\alpha_i \alpha_j} = \sum_{\overrightarrow{\kappa}} \hat{B}_{ij}(\overrightarrow{\kappa}, t) \tag{2.107}$$

$$\overline{\alpha_i u_j} = \sum_{\overrightarrow{\kappa}} \hat{C}_{ij}(\overrightarrow{\kappa}, t) \tag{2.108}$$

$$\overline{u_i \rho} = \sum_{\overrightarrow{\kappa}} \hat{D}_i(\overrightarrow{\kappa}, t) \tag{2.109}$$

$$\overline{\alpha_i \rho} = \sum_{\overrightarrow{\kappa}} \hat{E}_i(\overrightarrow{\kappa}, t) \tag{2.110}$$

$$\overline{u_i \beta} = \sum_{\overrightarrow{\kappa}} \hat{F}_i(\overrightarrow{\kappa}, t) \tag{2.111}$$

$$\overline{\alpha_i \beta} = \sum_{\overrightarrow{\kappa}} \hat{G}_i(\overrightarrow{\kappa}, t) \tag{2.112}$$

$$\overline{\beta \rho} = \sum_{\overrightarrow{\kappa}} \hat{H}(\overrightarrow{\kappa}, t) \tag{2.113}$$

$$\overline{\rho \rho} = \sum_{\overrightarrow{\kappa}} \hat{I}(\overrightarrow{\kappa}, t) \tag{2.114}$$

$$\overline{\beta \beta} = \sum_{\overrightarrow{\kappa}} \hat{J}(\overrightarrow{\kappa}, t) \tag{2.115}$$

These equations along with the wavenumber vector evolution equation make up the set of 65 ODEs necessary to solve Favre-averaged RDT. It is clear to see that

almost all the equations are interdependent on one another, therefore we must obtain a solution to the density-weighted turbulent kinetic energy using this averaging method. As in the previous averaging approach, a fourth order Runge-Kutta scheme is used to advance the solution in time.

C. Numerical Implementation and Validation

1. Numerical Implementation

In this section we will present the parameters and timescales that are utilized in this research. Previous work on rapid distortion theory has looked at all different types of flow deformation, but for this work we focus only on steady homogeneous shear deformation, where the mean velocity gradient is presented as:

$$\frac{\partial \overline{U_i}}{\partial x_j} = \begin{bmatrix} 0 & S & 0 \\ 0 & 0 & 0 \\ 0 & 0 & 0 \end{bmatrix} \tag{2.116}$$

We generate initial conditions for the real and imaginary covariances as well as the wavenumber vector in spectral space. We look at a collection of 6079 wavenumber vectors which are evenly distributed across the surface of a unit sphere. This approach is taken to ensure a statistical isotropic initial flow field. Initial velocity vectors are chosen such that they are normal to the wavenumber vectors to enforce initial incompressibility. To satisfy the dilatational initial conditions we make the amplitude and wavenumber vectors parallel to one another. We set the initial thermodynamic variables to standard values, density is set to $\overline{\rho} = 1.0$ and mean temperature is set to 300K.

Previous studies have shown that one of the most relevant parameters of com-

pressible RDT is the gradient Mach number:

$$M_g \equiv \frac{Sl}{\sqrt{\gamma R T_0}} \tag{2.117}$$

where R is the universal gas constant, T_0 is the initial temperature, and l is the initial characteristic length that is equivalent to the magnitude of the wavenumber vector. For low Mach number values the incompressible results are recovered(i.e. $M_g = 0.01$), whereas for high Mach number values we recover the Burger's limit results(i.e. $M_g = 2880$).

For this study we choose to examine two other parameters: (i) the initial turbulent Mach number M_t and (ii) the initial temperature fluctuation intensity T_s.

$$M_t = \frac{\sqrt{\overline{u_i' u_i'}}}{\sqrt{\gamma R T_0}} \tag{2.118}$$

$$T_s = \frac{\sqrt{\overline{T'T'}_0}}{\overline{T_0}} \tag{2.119}$$

These parameters are used to determine how initial thermodynamic and velocity fluctuations influence the evolution of the turbulent flow field. The parameter values for the different cases presented in this thesis are shown in Table I.

2. R-RDT Validation

Validation for R-RDT simulations against DNS results can be seen in previous works [10, 13]. Yu & Girimaji [10] demonstrate that the R-RDT equations capture the limiting cases of incompressible turbulence and pressure-released turbulence behavior accurately. At the limit of vanishingly small M_g, they show that this R-RDT formulation yields results identical to standard incompressible RDT results published, for example, in Pope [1]. At the other extreme, in the limit of very large Mach number, Yu & Girimaji show that R-RDT recovers known analytical solutions of

Table I. Case Parameter Values

Case	M_g	M_t	$T_s(\%)$	Case	M_g	M_t	$T_s(\%)$
1	5	0.1	0	16	30	0.5	0
2	5	0.5	0	17	30	1.0	0
3	5	1.0	0	18	30	2.0	0
4	5	2.0	0	19	30	0.1	1
5	5	0.1	1	20	30	0.1	5
6	5	0.1	5	21	30	0.1	10
7	5	0.1	10	22	67	0.1	0
8	15	0.1	0	23	67	0.5	0
9	15	0.5	0	24	67	1.0	0
10	15	1.0	0	25	67	2.0	0
11	15	2.0	0	26	67	0.1	1
12	15	0.1	1	27	67	0.1	5
13	15	0.1	5	28	67	0.1	10
14	15	0.1	10	29	0.01	0.1	0
15	30	0.1	0	30	2880	0.1	0

pressure-released turbulence.

In the work by Lavin [13] the R-RDT approach is validated against DNS results. Even though R-RDT only describes the linear processes of turbulence, it is shown that it still captures the flow physics in the rapid limit as seen in Figures 3 and 4. By examining the turbulent kinetic energy growth rate and the component of the anisotropy tensor in the direction of shearing, we see that R-RDT produces similar trends found in DNS results, but it is done with a small fraction of the computational effort required by DNS.

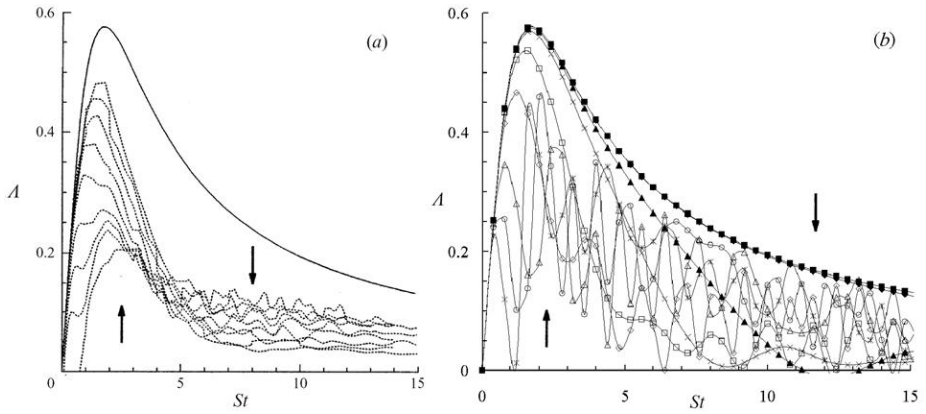

Fig. 3. Turbulent kinetic energy growth rate for varying gradient Mach numbers M_g. Plots are shown for (a)DNS (with solid line indicating Burgers limit and arrows showing direction of increasing gradient Mach number) and (b) R-RDT (values of M_g indicated as follows: $\star$: 0.72; $\circ$: 1.00; $\triangle$: 1.44; $\diamond$: 2.88; $\square$: 5.76; $\times$: 14.4; $\blacktriangle$: 28.8; $\blacklozenge$: 288; $\blacksquare$: 2880.)Produced by Tucker Lavin [13].

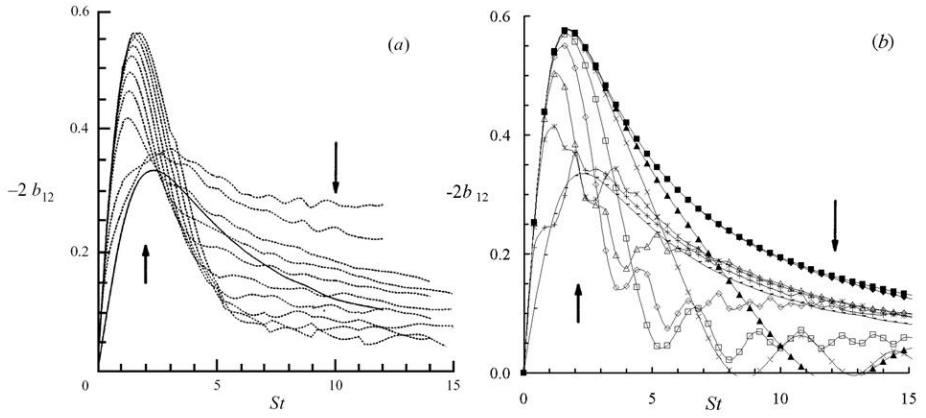

Fig. 4. b_{12} anisotropy component of initially-incompressible homogeneous turbulence in pure shear for varying gradient Mach numbers M_g.Plots are shown for (a)DNS (with solid line indicating Burgers limit and arrows showing direction of increasing gradient Mach number) and (b) R-RDT (values of M_g indicated as follows: $\star$: 0.72; $\circ$: 1.00; $\triangle$: 1.44; $\diamond$: 2.88; $\square$: 5.76; $\times$: 14.4; $\blacktriangle$: 28.8; $\blacklozenge$: 288; $\blacksquare$: 2880.)Produced by Tucker Lavin [13].

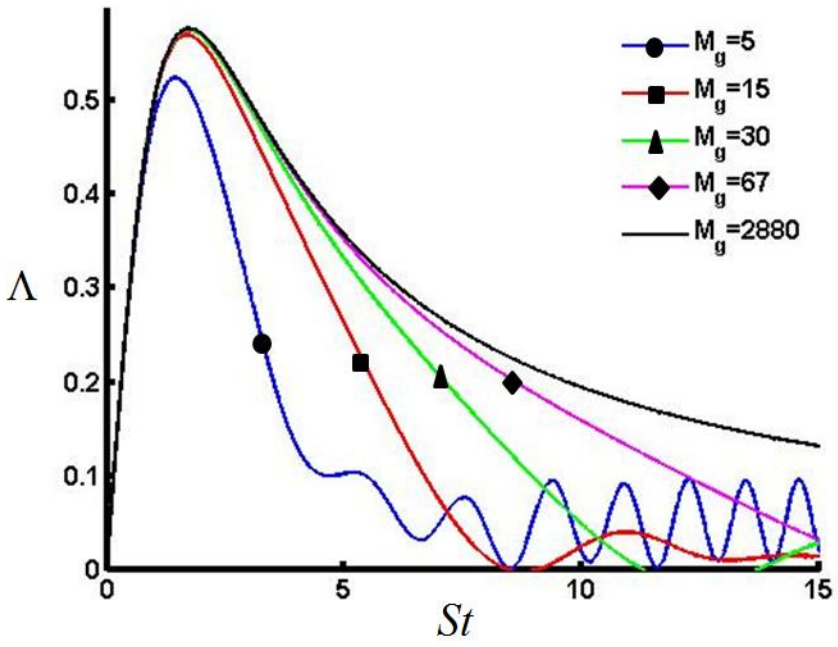

Fig. 5. Evolution of turbulent kinetic energy for varying initial gradient Mach numbers(M_g).

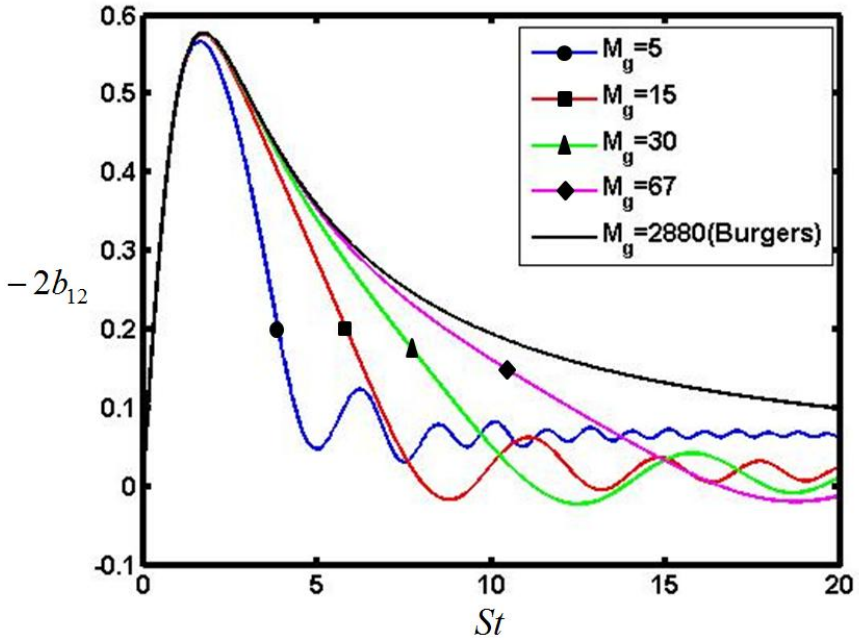

Fig. 6. b_{12} anisotropy component of initially-incompressible homogeneous turbulence in pure shear for varying gradient Mach numbers M_g.

3. F-RDT Validation

Preliminary validation for this approach was first seen in Lavin [13] where comparison of F-RDT and R-RDT results showed tremendous agreement. Lavin explains this similarity by proving that the velocity mean and fluctuating components yield the same values for both averaging approaches. As a result, the covariance of both techniques are the same, leading to matching turbulent kinetic energy and internal energy growth. Turning to Figure 5, our results from the F-RDT approach produces the same turbulent kinetic energy growth rate pattern which is seen in previous R-RDT and DNS studies. In Figure 6 we present the component of the anisotropy tensor in the direction of shearing. By comparing this Figure 6 with Figure 4 we see that the same basic trends are present. F-RDT even captures the trend seen in DNS of the anisotropy tensor where the larger initial Mach numbers dip further and oscillate

after their maximum value. At this point, we can state that F-RDT performs at the same level as R-RDT simulations. In Chapter IV of this thesis we present why F-RDT is the superior choice in approaches when examining the linear processes found in turbulence. Unless otherwise stated, only F-RDT will results will be presented from this point onward. The parameters values for each case are presented in Table I.

CHAPTER III

CHARACTERIZATION OF THREE-STAGE BEHAVIOR

It can be seen from previous works [10, 11, 12, 13] that key flow statistics - kinetic energy, Reynolds stresses - of compressible homogeneous shear turbulence exhibit a multistage temporal growth: (i) early time, (ii) intermediate time and (iii) asymptotic state. The turbulent kinetic energy has been a key property of study in compressible RDT [10, 11, 12, 13]. The three stages can also be labeled according to the growth rate of kinetic energy. The three regimes are: (1) rapid growth stage equivalent to growth exhibited by the pressure-released case, (2) a stabilization stage where energy growth is nearly zero, (3) asymptotic regime of growth similar to incompressible flows. The most complete explanation, to date, of the multi-stage evolution of rapidly sheared compressible turbulence is provided by Cambon and co-workers in a series of articles [3, 9]. Using a semi-analytical investigation, these authors provide a preliminary explanation for the observed behavior at three distinct time regimes. The authors also clearly distinguish the differences between compressible sheared and strained flows. It is also shown the asymptotic linear effects may be independent of initial Mach number, whereas the non-linear processes exhibit a stronger dependence. There is a clear demonstration in these papers [3, 9] that the stabilizing effect of compressibility in shear flows can be adequately explained with the linear Rapid Distortion Theory. The stabilization is attributed to the feed-back of the dilatational disturbances upon the solenoidal field [13].

In this chapter, we investigate the stabilization process in greater detail. We seek to understand the three-stage behavior in terms of the changing role of pressure in each regime. Important contributions in this regard has been made by Livescu [14] who focuses on the level of anisotropy at different regimes. The focus of this work is

on the mechanisms in different stages. To further demarcate the three-regimes, we examine the RDT evolution in three different timescales. Throughout this chapter (unless otherwise stated) only $M_g(0)$ is varied and $M_t(0)$ is held constant at 0.1 for different runs.

A. Three-Stage Behavior in Different Timescales

The three timescales used in the investigation are: (i) shear time, (ii) acoustic time (at/l_0), and (iii) mixed time ($\sqrt{\frac{a}{l_o}}t$). We choose to view our results in this manner because each timescale highlights different aspects of flow physics. First we examine the evolution of kinetic energy in various timescales:

$$k = \frac{1}{2}\overline{\rho u_i' u_i'} \tag{3.1}$$

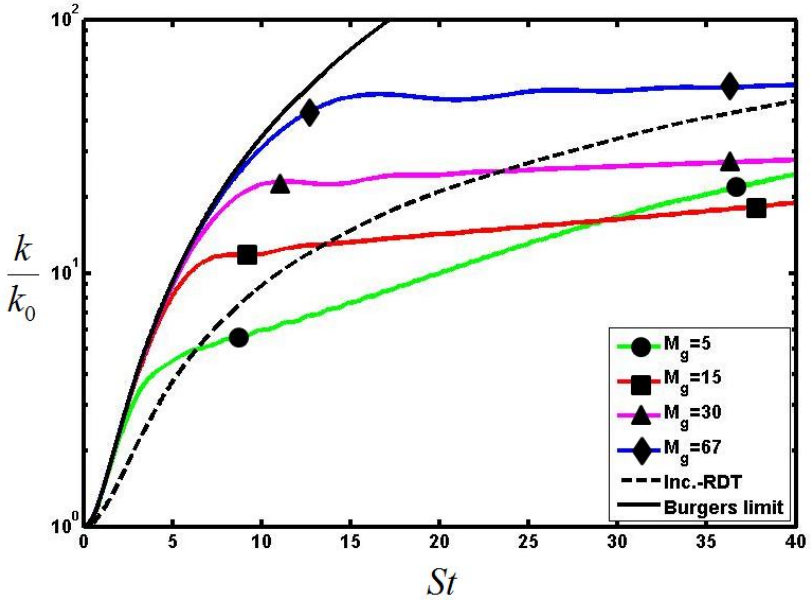

Fig. 7. Evolution of normalized turbulent kinetic energy for varying initial gradient Mach numbers(M_g) as seen in shear time for initial $M_t = 0.1$.

1. Shear Time

In previous studies, the majority of temporal evolution results are presented in shear time (St) since the timescale is a directly related to the total shear applied to the system. In this timescale the transition between stage 1 and Stage 2 is most evident. This transition represents the 'peel-off' of kinetic energy value from Burger's limit to the stabilization regime, as can be seen in Figure 7. These transition times are consistent with that seen in Simone et. al.[9].

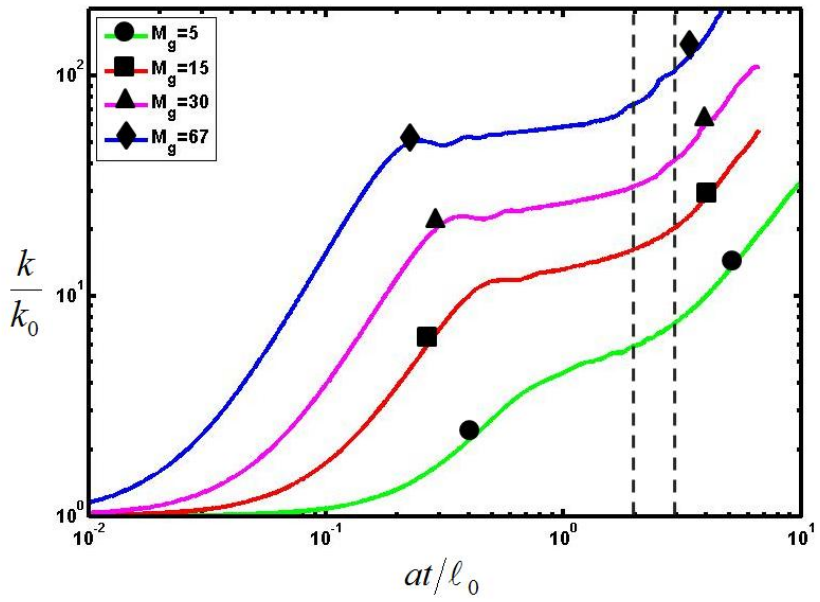

Fig. 8. Evolution of normalized turbulent kinetic energy for varying initial gradient Mach numbers(M_g) as seen in acoustic time for initial $M_t = 0.1$.

2. Acoustic Time

The use of acoustic timescales ($at = t * \sqrt{\gamma R T_0}$) to display the multistage growth of properties in compressible flow at the rapid distortion limit was first done in Lavin [13] for the case of R-RDT. In Figure 8, we present F-RDT turbulent kinetic energy

evolution in acoustic time for different gradient Mach numbers. The acoustic timescale has the advantage of clearly displaying the three-stage growth of turbulent kinetic energy. Another advantage of the acoustic timescale is the clear demonstration of the onset of the third regime. Figure 8 also shows the third and final regime is reached at approximately two or three acoustic time units for all M_g cases. Again, further study is presented later to support this observation.

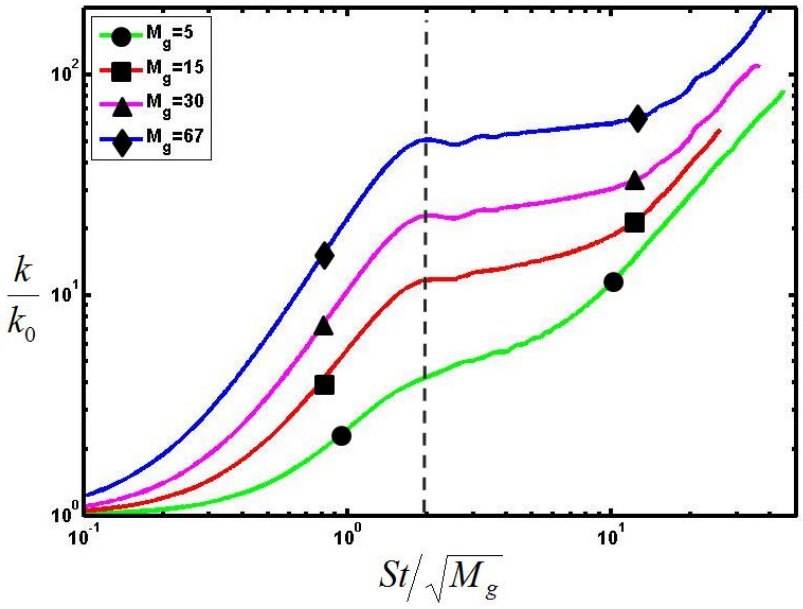

Fig. 9. Evolution of normalized turbulent kinetic energy for varying initial gradient Mach numbers(M_g) as seen in mixed time for initial $M_t = 0.1$.

3. Mixed Time

The mixed timescale is the geometric average of the shear and acoustic time scales ($\frac{St}{\sqrt{M_g}}$). We introduced this timescale as another option to clearly display the three-stage turbulent kinetic energy evolution. The main benefit of this normalization is that the onset of regime 2 is at an identical time for all Mach numbers considered.

4. Regimes of Evolution

Inspections of Figures 8 and 9 show the approximate time demarcations between the three regimes of behavior.

Regime 1: $0 < St < 1 - 2\sqrt{M_g}$

Regime 2: $1 - 2\sqrt{M_g} < at < 1 - 3$

Regime 3: $at > 3$

The exact demarcation between the various regimes and the physics within each regime will be addressed later.

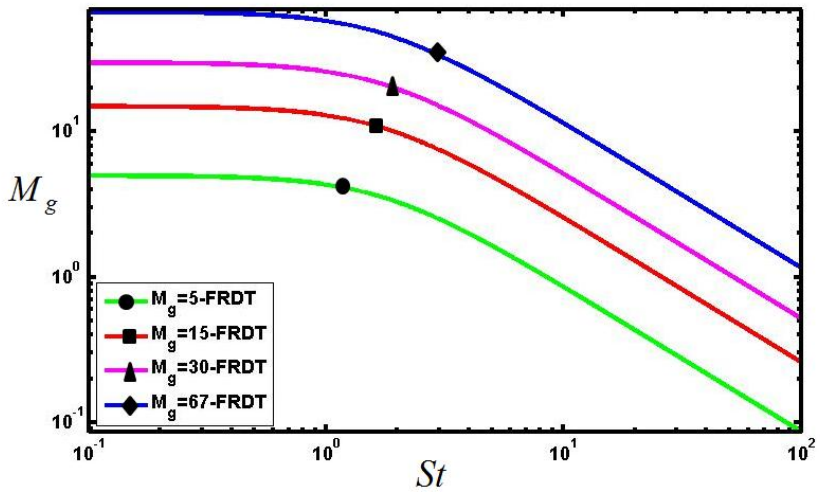

Fig. 10. Evolution of gradient Mach number in shear time-scale.

B. Evolution of Gradient and Turbulent Mach Numbers

As the turbulence field evolves from its initial conditions, both M_g (gradient Mach number) and M_t (turbulent Mach number) evolve from their initial values. It is instructive to examine the evolution of these Mach numbers as a function of time. In Figures 10, 11 and 12, the evolution of the gradient Mach number is shown in different time scales. By examining the evolution of M_g in shear time, it is clear that

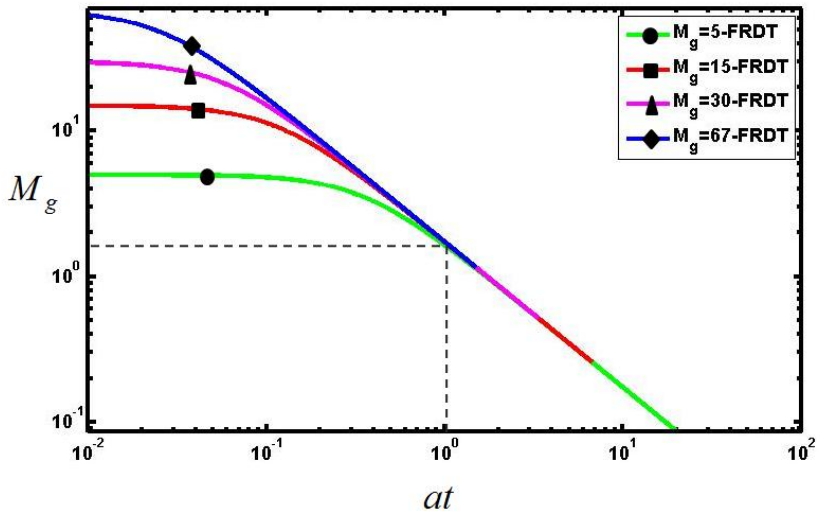

Fig. 11. Evolution of gradient Mach number in acoustic time-scale.

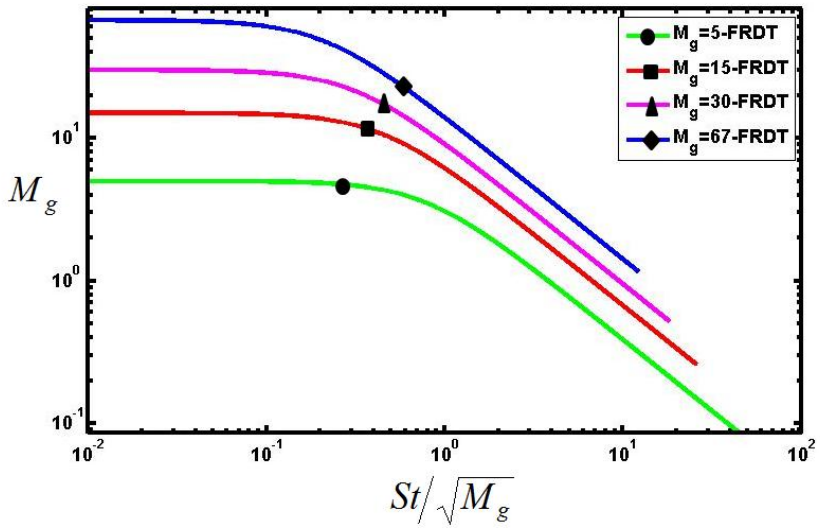

Fig. 12. Evolution of gradient Mach number in mixed time-scale.

within one shear time, the initial gradient Mach number value begins to significantly decrease. It is very interesting to note that within one acoustic time (Fig. 11), the gradient Mach number is nearly one for all initial M_g values. After one acoustic time, the evolution of the gradient Mach number is confined to the path laid out in Figure 11. From these figures, it is possible to determine the value range of the gradient Mach number in each regime.

In Figures 13, 14, and 15 the evolution of the initial turbulent Mach number is presented in the different timescales. In shear time, it is important to note that after four shear times, the growth of all initial turbulent Mach numbers decreases significantly. In acoustic time, the 3-regime evolution is clearly seen, but no significant alignment of all cases is present. The evolution of the initial turbulent Mach number is best displayed in mixed time due to the fact that both the 3-regime growth is evident and all runs align where the initial values begin to show significant growth.

C. Physics of Different Regimes

The objective in this section is to perform a careful analysis of the various physical processes in each regime. We are especially interested in the changing role of pressure. To examine the physical processes we study the linearized Reynolds-Stress evolution equation (e.g. Pope [1]).

$$\frac{d\overline{\rho u_i{}^{"} u_j{}^{"}}}{dt} = P_{ij} + \Pi_{ij}{}^{(r)} \tag{3.2}$$

where P_{ij} is the production tensor and $\Pi_{ij}{}^{(r)}$ is the rapid pressure-strain correlation tensor. In linear analysis, the evolution of the Reynolds-stresses is influenced purely by the inertial effects (P_{ij}) and the pressure effects ($\Pi_{ij}{}^{(r)}$). As mention in the introduction to this thesis, the rapid pressure-strain correlation is one of the terms that require improved closure modeling. In this section we will determine the role of

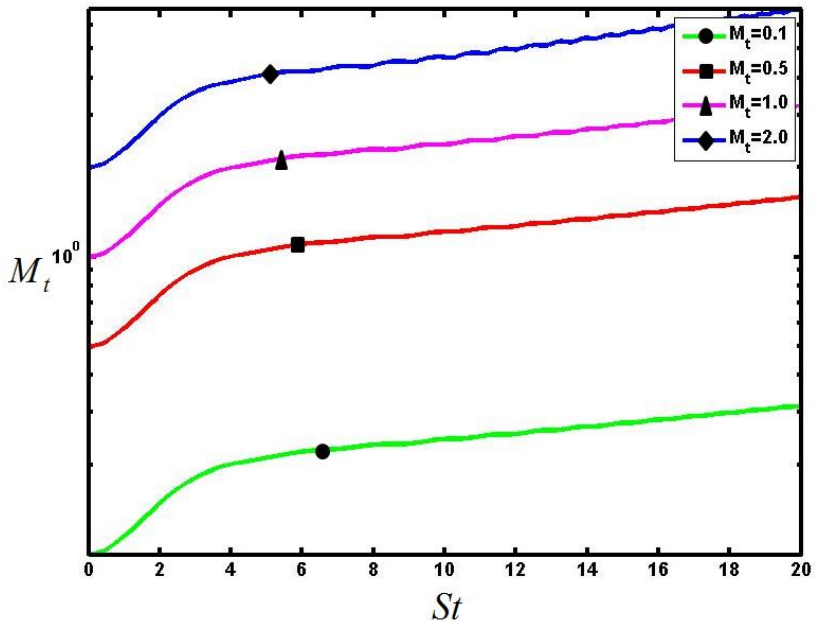

Fig. 13. Evolution of turbulent Mach number in shear time-scale for zero initial temperature fluctuations and an initial $M_g = 5$.

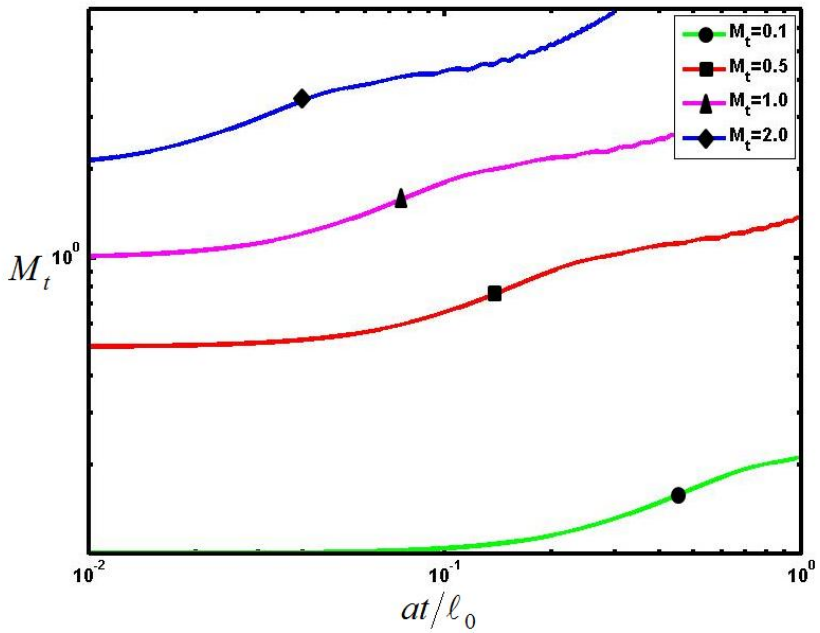

Fig. 14. Evolution of turbulent Mach number in acoustic time-scale for zero initial temperature fluctuations and an initial $M_g = 5$.

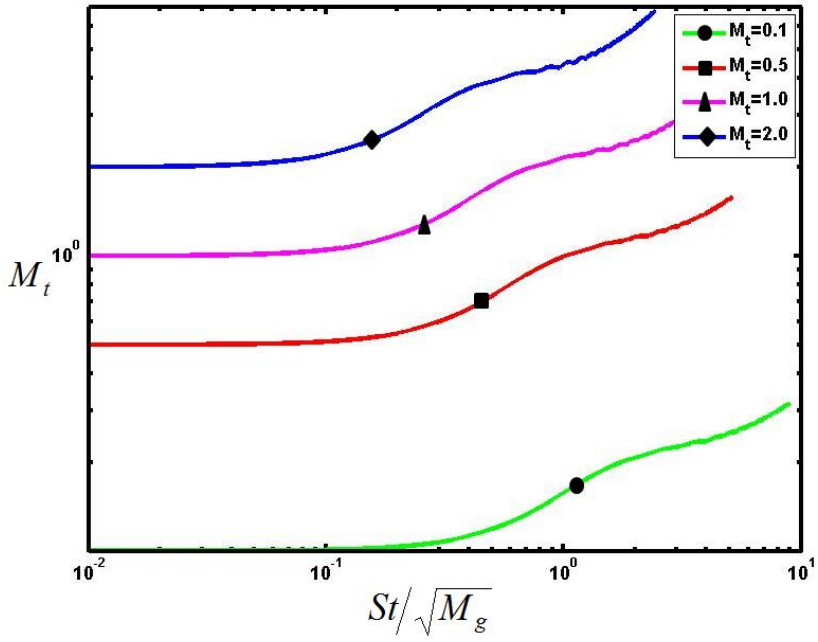

Fig. 15. Evolution of turbulent Mach number in mixed time-scale for zero initial temperature fluctuations and an initial $M_g = 5$.

the rapid pressure-strain correlation in each regime by studying the evolution of the production tensor and the time rate of change of the Reynolds stresses.

We first present the evolution of Reynolds-stress growth rate and production in all three time scales in Figures 16, 17 and 18. In all timescales, the three-regime evolution is easily seen. Once again each timescale highlights different features. In Figure 16 which displays the results in shear time, we notice how the smaller initial gradient Mach number cases seem to "peel-off" a high Mach number path, similar in manner to the first regime in the evolution of turbulent kinetic energy. We present the evolutions in acoustic time in Figure 17 where we can see that regardless of the initial gradient Mach number, the evolution of production and the growth rate of the Reynolds stresses all evolve along the same path in the final regime. For the mixed timescale, seen in Figure 18, all the maximum peaks align at one mixed time unit. In

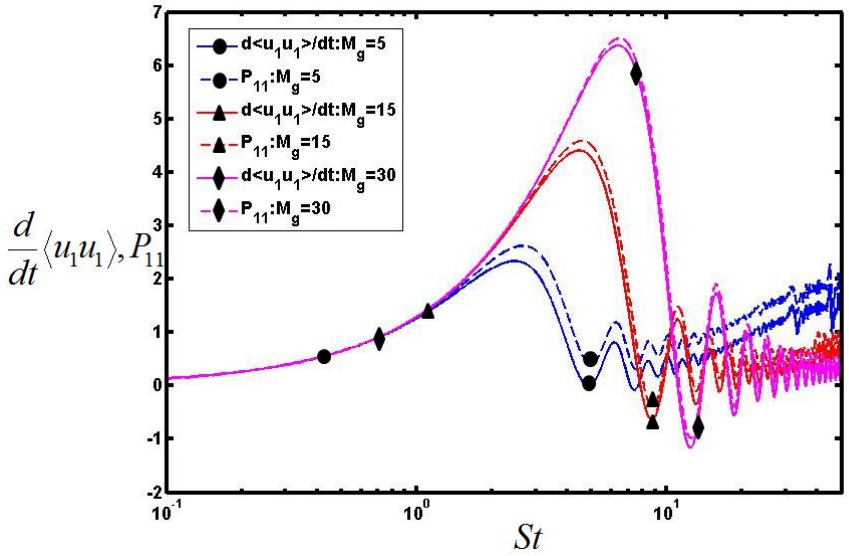

Fig. 16. Evolution of production and time rate of change of reynolds stresses in shear time-scale for $M_g = 5$.

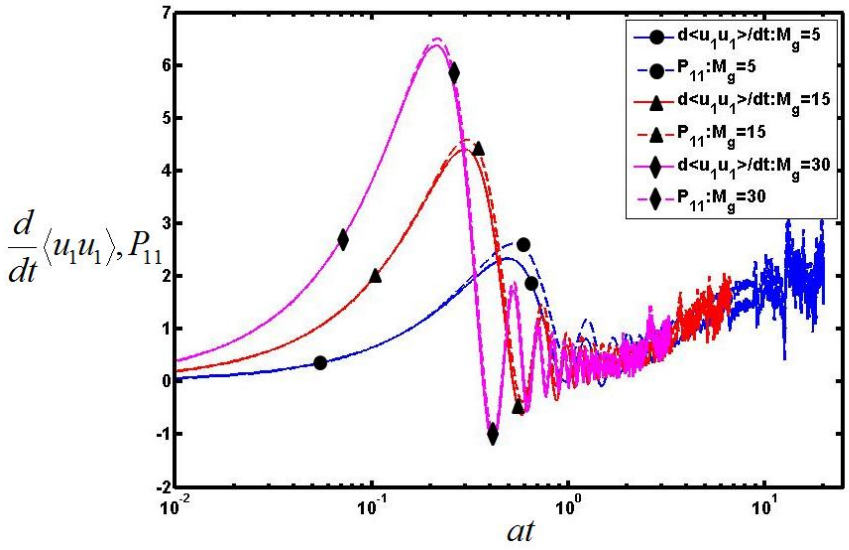

Fig. 17. Evolution of production and time rate of change of reynolds stresses in acoustic time-scale for $M_g = 5$.

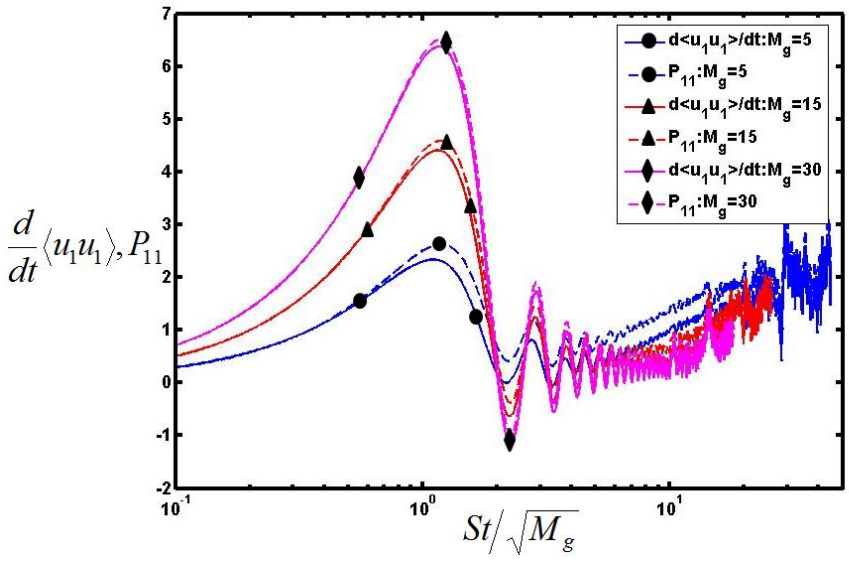

Fig. 18. Evolution of production and time rate of change of reynolds stresses in mixed time-scale for $M_g = 5$.

order to determine the role of pressure in each regime, we must examine each regime individually.

1. Regime 1

When examining the first regime of production evolution and Reynolds-stress growth, the nature of pressure is most clearly seen by studying the P_{11} and $\overline{u_1 u_1}$ components. In Figure 19, the production and Reynolds-stress growth lines are nearly identical throughout the majority of the first regime. Using Equation 3.2 we can surmise that the role of the pressure strain correlation, and therefore the role of pressure itself, is negligible in this regime. We see that before we get to a mixed time of 1, the production and Reynolds-stress growth lines start to diverge for the smaller initial gradient mach numbers. This separation indicates that pressure begins to play a more significant role in the flow field physics. The moment of separation of production and Reynolds-stress growth coincides with the "peel-off" seen in the first

regime of turbulent kinetic energy evolution. Thus, we can conclude that in the first regime, the effect of advection dominates pressure yielding a behavior identical to the pressure-released or Burger's limit turbulence.

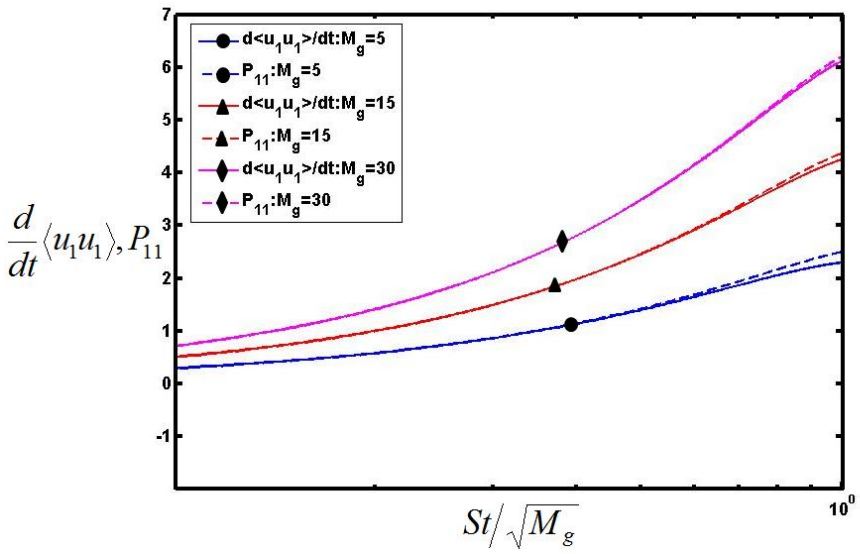

Fig. 19. Evolution of production and time rate of change of Reynolds stresses in mixed time-scale during the first stage of evolution.

By examining other statisical quantities of the flow field we can gain a better understanding of the physics involved in the first regime of growth. In Figure 20, the evolution of the pressure fluctuations moment is presented in mixed time. As expected from the examination of Figure 19 the fluctuating pressure experiences zero growth during this regime. Towards the end of the first regime the fluctuating pressure obtains non-zero values but they are still small. The study the evolution of the dilatational kinetic energy and the internal energy is shown in Figures 21 & 22. The dilatational kinentic energy remains at a constant non-zero value throughout the majority of the first regime where as the internal energy obtains a non-zero value toward the end of this regime. It is clear that the partition between these energies heavily favors the dilatational kinetic energy.

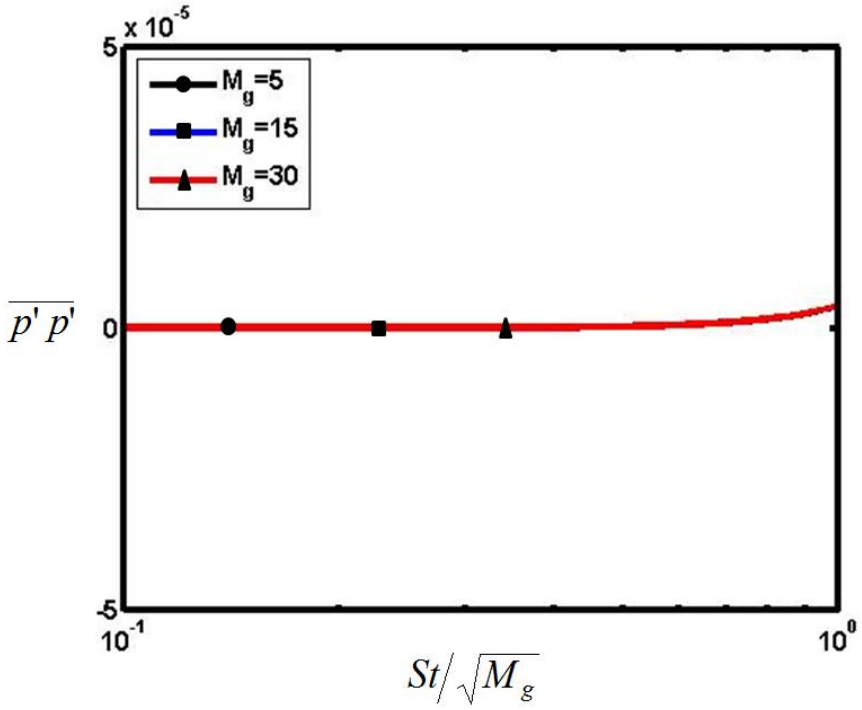

Fig. 20. Evolution of fluctuating pressure moment in mixed time-scale during the first stage of evolution.

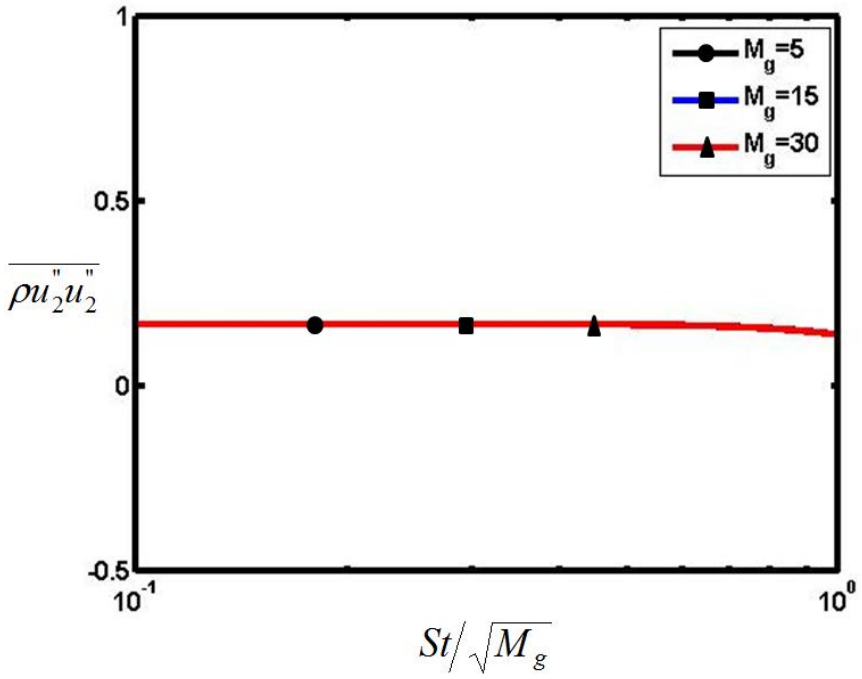

Fig. 21. Evolution of dilatational kinetic energy in mixed time-scale during the first stage of evolution.

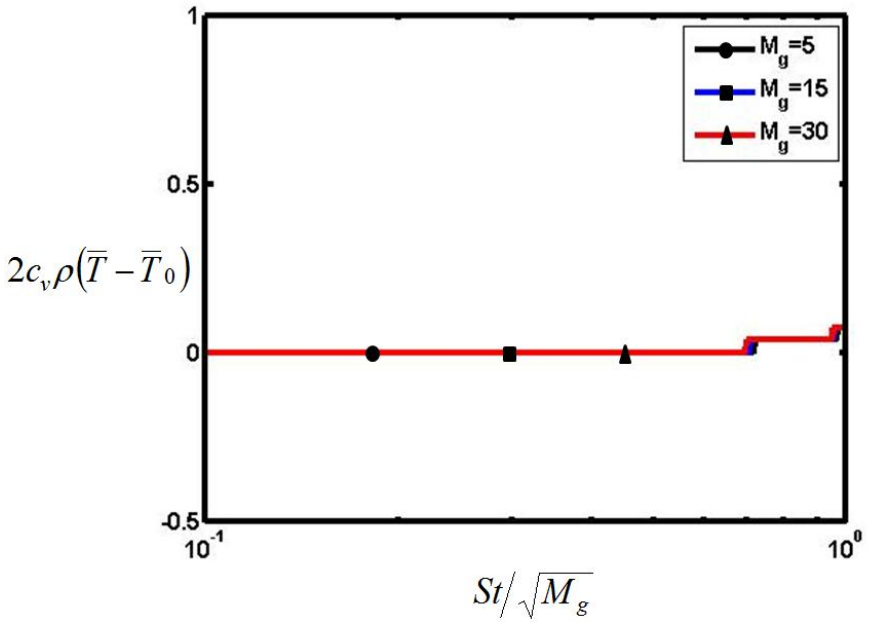

Fig. 22. Evolution of the increment in thermal energy in mixed time-scale during the first stage of evolution.

2. Regime 2

For regime 2, the overall picture is best demonstrated by examining P_{12} and the growth of $\overline{u_1 u_2}$. The evolution of these quantities is shown in Figure 23. Unlike in the previous regime, the production and Reynolds-stress growth rate no longer coincide. Although the magnitude of production is very large, the $\overline{u_1 u_2}$ growth rate oscillates about zero, implying that the overall Reynolds-stress growth is zero during this regime. Again, referring to Equation 3.2, we can infer that the pressure-strain correlation term is working to nullify the production. Relating this back to the turbulent kinetic energy evolution, this regime where pressure fights the inertial physics coincides with the stabilization regime. Since there is non-zero growth in the final regime, the second regime acts a buffer region between negligible pressure effects in the first regime and the final role of pressure in the third regime.

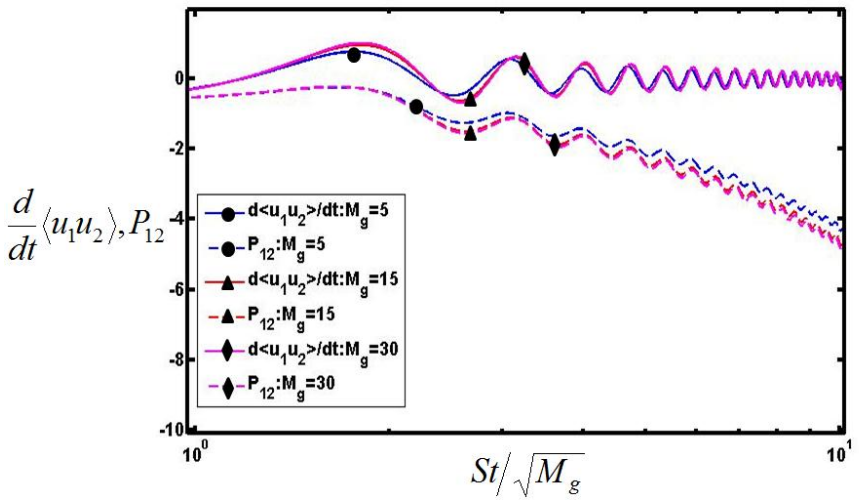

Fig. 23. Evolution of production and time rate of change of Reynolds stresses in mixed time-scale during the second stage of evolution.

Again, we examine the same flow field statistical quantities as regime 1 to understand more of the physics associated with this regime. In Figure 24, the evolution of the fluctutating pressure moment is displayed for the second regime. In this regime, the fluctuating pressure experiences oscillatory growth. By comparing Figures 23 & 24 we see that the fluctuating pressure moment and production term are oscillating in phase to one another. The figures support our previous conclusion that pressure is working against production to stabilize the growth of the Reynolds-stresses by showing that production evolves toward more negative values and the pressure fluctuating moment evolves toward more positive values.

Examining the dilational kinetic energy and the increase in thermal energy in Figures 25 and 26, we notice that these statistical quantities move away from their initial values.

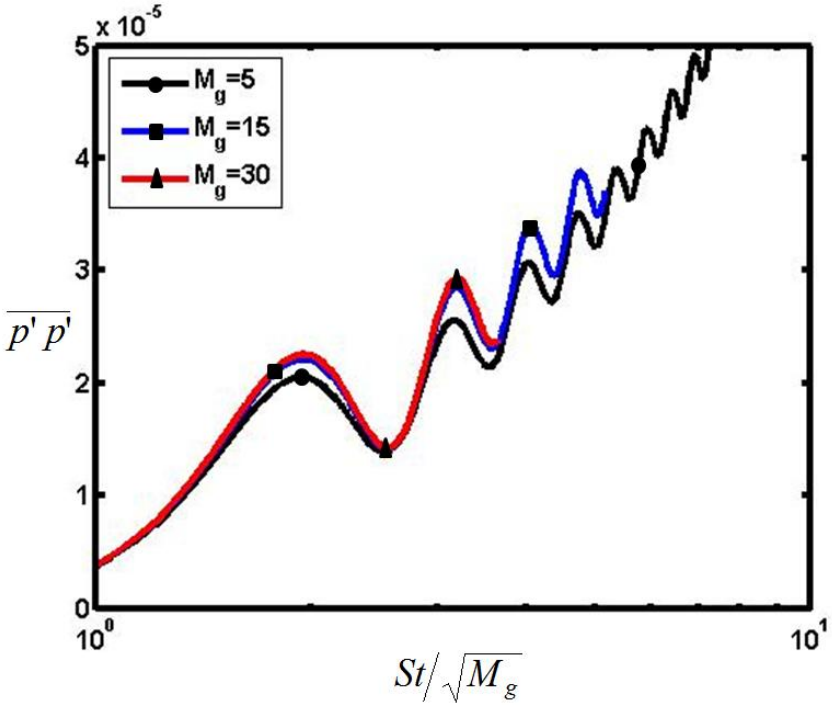

Fig. 24. Evolution of fluctuating pressure moment in mixed time-scale during the second stage of evolution.

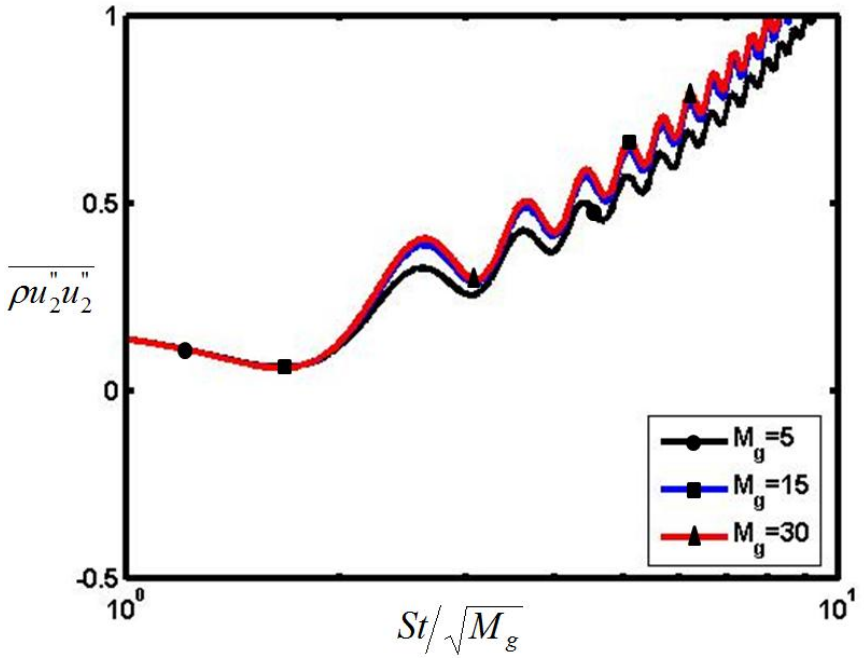

Fig. 25. Evolution of dilatational kinetic energy in mixed time-scale during the second stage of evolution.

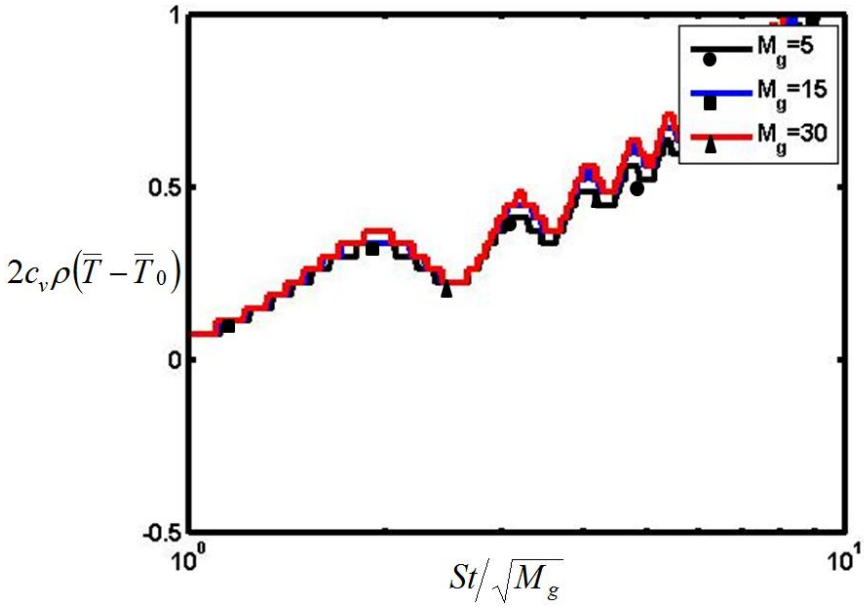

Fig. 26. Evolution of the increment in thermal energy in mixed time-scale during the second stage of evolution.

3. Regime 3

The final regime of evolution is best examined in terms of $P_{1,1}$ and $\Pi_{1,1}$ as seen in Figures 27 & 28. The most important feature is that the behavior of all gradient mach number cases is nearly identical. This is in complete contrast to the previous regimes in which $M_g(0)$ played a significant role. The collapse of the results is also consistent with the fact that the $M_g(t)$ at these times is independent of $M_g(0)$. It is also seen that this behavior is similar to that of incompressible flows as seen in Figure 29. In summary, the pressure-strain correlation in this regime is similar to that of incompressible turbulence. This finding lends quantitative support to the conclusions of Simone et. al. [9].

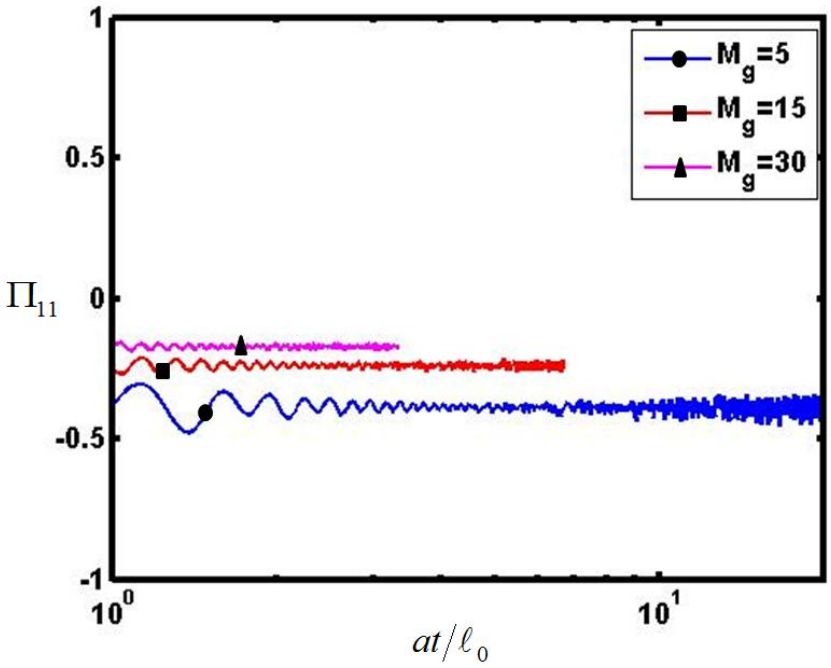

Fig. 27. Evolution of rapid pressure-strain correlation term in mixed time-scale during the third stage of evolution.

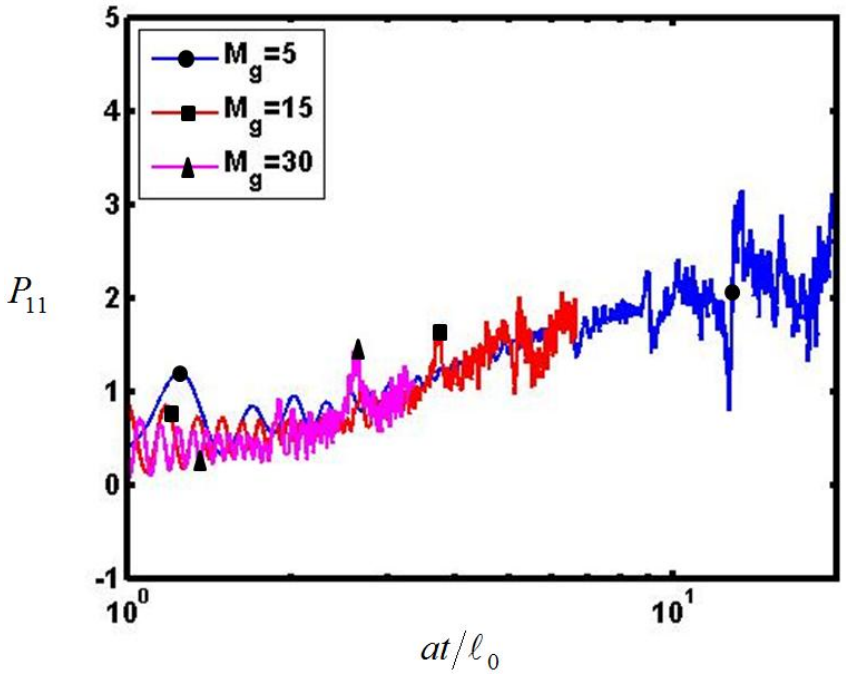

Fig. 28. Evolution of the production term in mixed time-scale during the third stage of evolution.

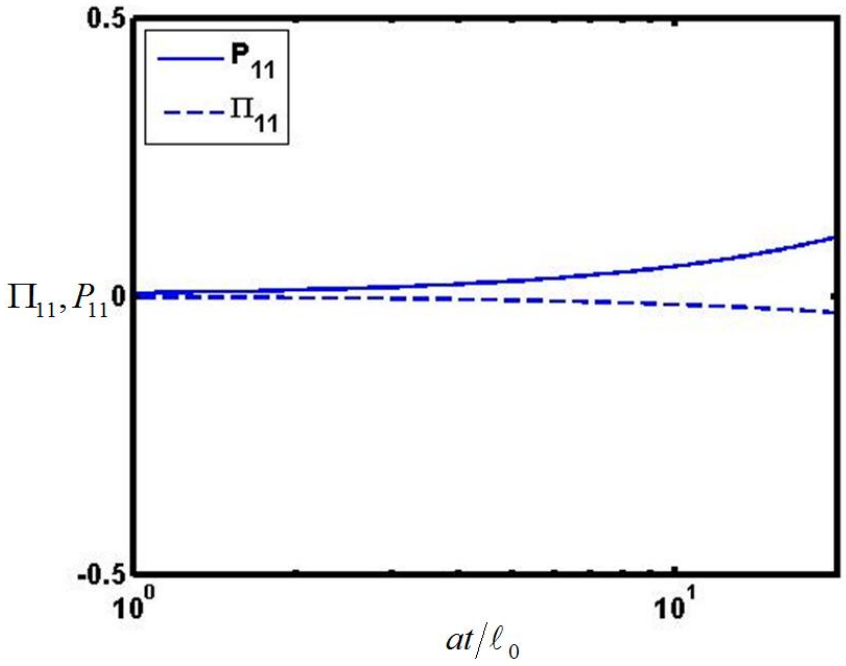

Fig. 29. Evolution of rapid pressure-strain correlation and production terms in the incompressible limit, shown in mixed time-scale.

To gain a greater understanding of the third regime, we look at the evolution of the pressure fluctuations. We previously discussed the oscillatory nature of the evolution of the pressure fluctuations in the second regime. This implies that the pressure fluctuations in the second regime are governed by the wave equation. In the third regime however, we observed that the production and rapid pressure-strain correlation terms evolve in a manner similar to the incompressible limit. This suggests that the pressure fluctuations are governed by the rapid part of Poisson's equation:

$$\nabla^2 p^{(r)} = -2\rho \frac{\partial \tilde{U}_i}{\partial x_j} \frac{\partial u_j^{"}}{\partial x_i} \tag{3.3}$$

We examine the evolution of Poisson pressure in several different M_g cases in Figure 30. We note that even though the Poisson pressure fluctuations are large initially, within three acoustic times, Poisson pressure has evolved to near zero values. With our previous conclusions in mind, we plot the evolution of the pressure fluctuations from the compressible RDT method, governed by Eq. 2.75, expecting all cases to tend toward a near zero value. However, we discover that the compressible pressure fluctuation settle to a value of unity as seen in Figure 31. We note that the compressible fluctuations settle about a constant value after 2-3 acoustic times, which shows agreement with Poisson pressure agreement. To finish our analysis we must determine what causes the compressible pressure fluctuations to settle at unity and not zero.

We previously deduced that the wave equation governs the second regime of evolution for all flow field properties. We also mentioned that the frequency of the wave oscillations increases in time and the oscillations continue into the third regime of evolution. Based on this understanding, it is evident that there are still residual wave effects occurring in the third regime where Poisson's equation dominates as the governing equation. Following this logic, we subtract the pressure fluctuations pro-

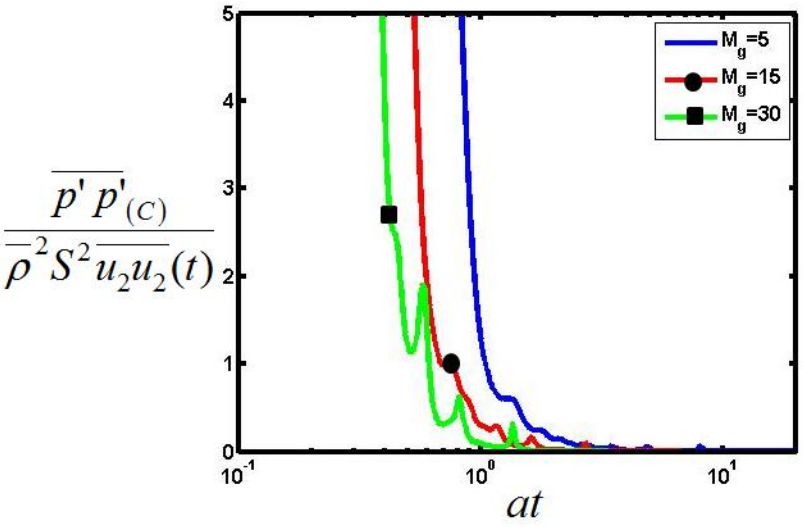

Fig. 30. Evolution of Poisson pressure fluctuations in the acoustic time-scale.

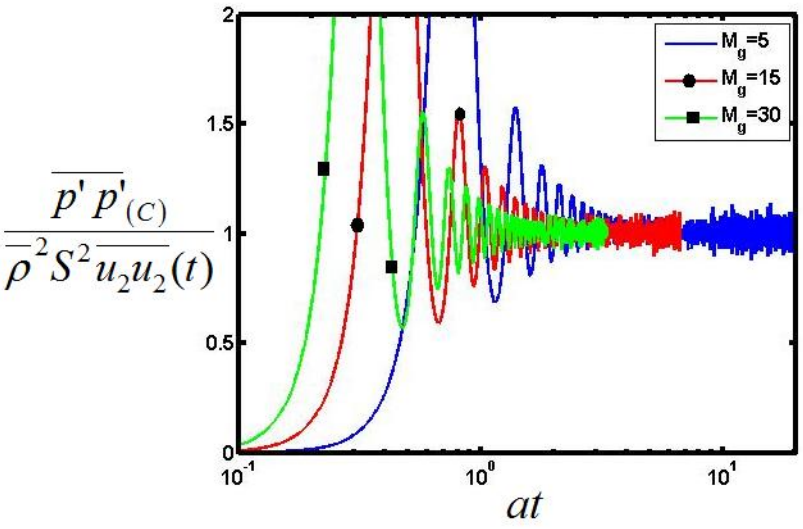

Fig. 31. Evolution of compressible pressure fluctuations in the acoustic time-scale.

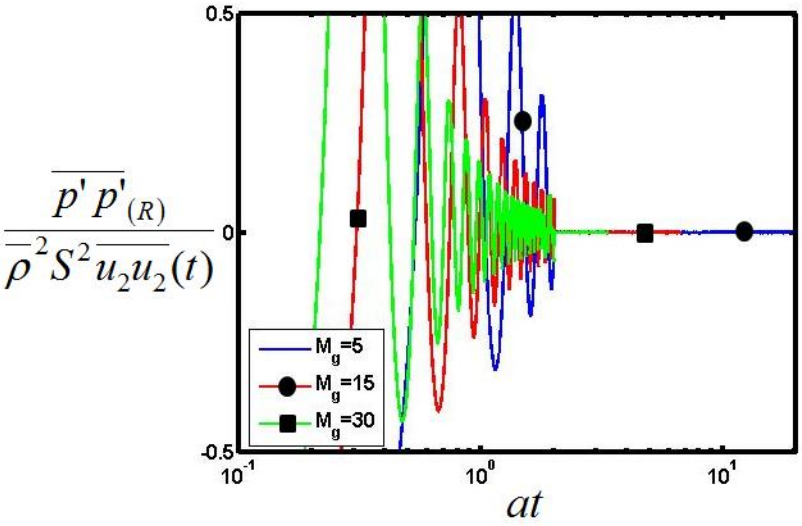

Fig. 32. Evolution of residial pressure fluctuations in the acoustic time-scale.

duced by Poisson's equation from the compressible pressure fluctuations to produce the residual pressure fluctuations:

$$\overline{p'p'}_{(res.)} = \frac{\overline{p'p'}_{(c)} - \overline{p'p'}_{(w)}}{\overline{\rho}^2 \gamma R T \overline{u_2'' u_2''}(t)} \tag{3.4}$$

We find agreement between the residual pressure fluctuations produced by the compressible RDT method and the Poisson equation approach by comparing Figure 30 and Figure 32. It can be deduced from this agreement that the third regime of evolution is governed by Poisson's equation as in incompressible fluid flow but it still maintains residual wave pressure produced in the second regime.

CHAPTER IV

POLYTROPIC COEFFICIENT

Earlier, we developed two different compressible RDT approaches, Reynolds-averaged and Favre-averaged, for homogeneous shear flow and presented validation of both approaches against DNS results. We claimed the F-RDT approach was more accurate for thermodynamic quantities. We now present evidence of this statement until this section.

The validation of the F-RDT approach for thermodynamic fluctuations is given by examining the evolution of the polytropic coefficient for different initial turbulent Mach numbers. The polytropic coefficient quantifies the relationship between the pressure and density fluctuations:

$$n \equiv \sqrt{\frac{\overline{p'p'}/\overline{p}^2}{\overline{\rho'\rho'}/\overline{\rho}^2}} \tag{4.1}$$

Blaisdell [6] clearly demonstrates using DNS data that the polytropic coefficient shoud be approximately equal to the specific heat ratio of the medium (1.4). In Figure 33 the evolution of the polytropic coefficient is shown for several initial turbulent Mach numbers. Using R-RDT computations, as the value of the initial turbulent Mach number increases, the polytropic coefficient tends away from the expected value. In fact, it attains values close to zero close to zero at late times. Clearly this behavior is unphysical. In Figure 34 the FRDT results for the polytropic coefficient of different initial turbulent Mach numbers are presented. Unlike the R-RDT results, the F-RDT results remain close to the expected value of 1.4 regardless of the magnitude of the initial turbulent Mach number. Thus, F-RDT is the more appropriate choice for examining compressible RDT for homogeneous shear flows because it captures the thermodynamic aspects of flow physics better than R-RDT.

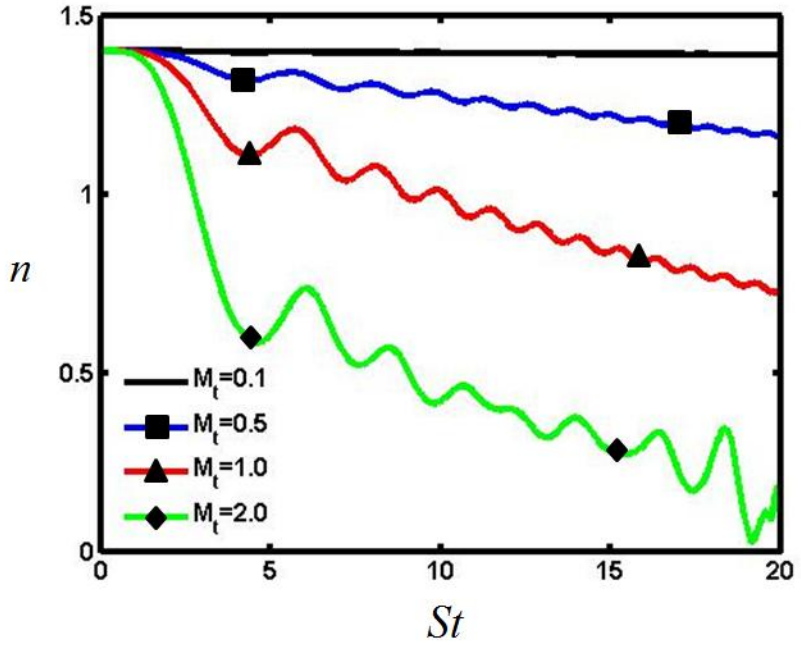

Fig. 33. Evolution of Averaged Polytropic coefficent for large initial turbulent Mach numbers for $M_g = 5$ via R-RDT approach.

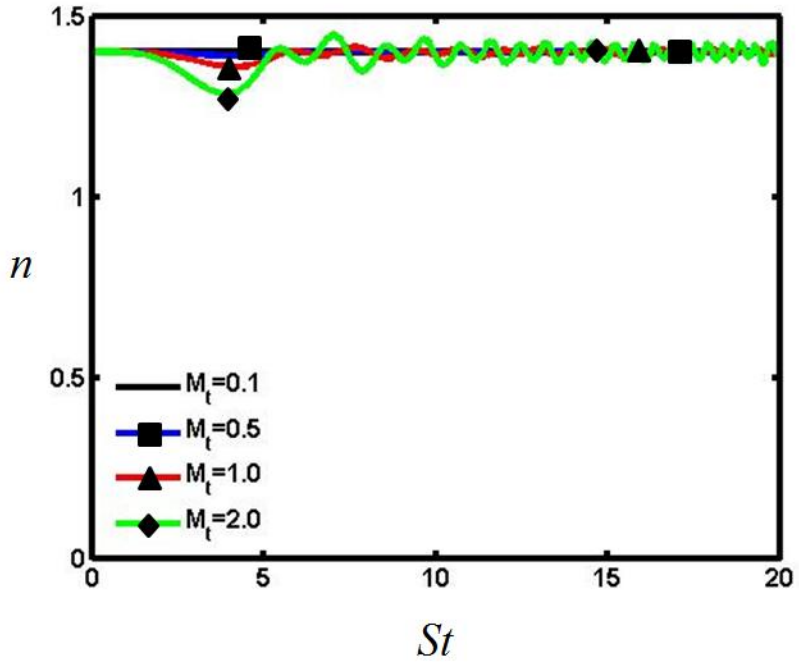

Fig. 34. Evolution of Averaged Polytropic coefficent for large initial turbulent Mach numbers for $M_g = 5$ via F-RDT approach.

CHAPTER V

EFFECT OF THERMODYNAMIC FLUCTUATIONS

All previous studies involving the R-RDT and F-RDT approaches have all examined simulations where all the thermodynamic fluctuating quantities were initially zero and the initial turbulent Mach number was small(0.004)[10, 13]. However, in realistic applications thermodynamic fluctuations can be substantial. In this chapter we investigate the effect of initial thermodynamic and velocity fluctuations on the evolution of the flow field statistics.

A. Kinetic Energy

We already presented a detailed analysis of the three-regime evolution of turbulent kinetic energy in Chapter III. Now we attempt to understand the effect of initial temperature fluctuations and the initial turbulent Mach number on the three-regime evolution.

1. Initial Temperature Fluctuation Intensity

We now investigate the influence of initial thermodynamic fluctuations. The results shown in Figure 35 are cases for which the initial temperature fluctuations are 0, 1, 5 and 10 percent of the initial mean temperature value. It is evident from Figure 35 that small temperature fluctuations have very little influence on the three regime evolution. However large initial temperature fluctuations heavily influence the evolution of the flow field by delaying the onset of the second regime where the growth stabilization occurs. This effect is important because it implies that large initial temperature fluctuations have the same influence as increasing the initial gradient Mach number. Since all the thermodynamic variables are linked by the state equation of an ideal

gas, it can be inferred initial pressure fluctuations will have similar influences on the evolution of the turbulent kinetic energy.

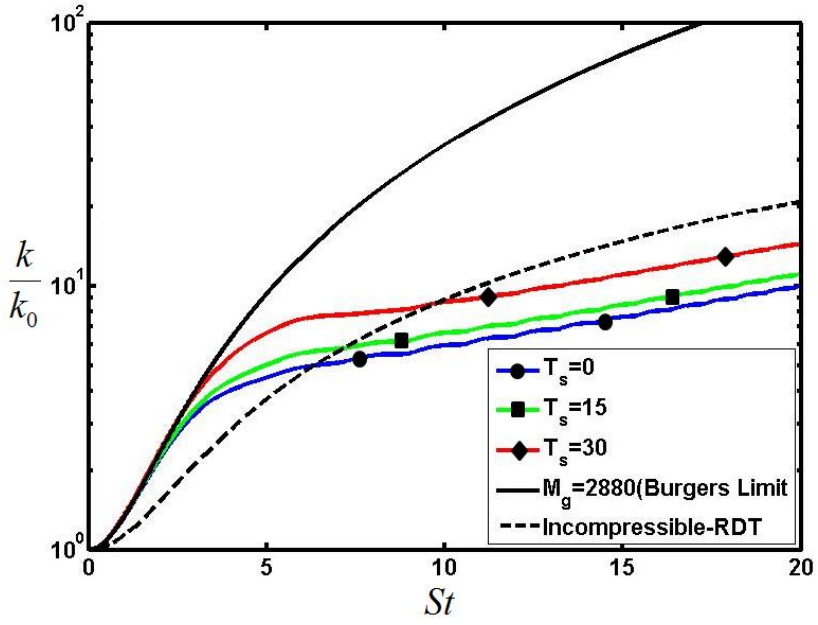

Fig. 35. Evolution of Turbulent Kinetic Energy for different initial temperature fluctuations for $M_g(0) = 5$ and $M_t(0) = 0.1$.

2. Initial Turbulent Mach Number

The effect of the initial velocity fluctuations is investigated by varying the initial turbulent Mach number, M_t. These results are shown in Figure 36. It is clear that the influence of the initial turbulent Mach number on the evolution of turbulent kinetic energy is very weak. Even large initial M_t values have very little affect on the three-regime evolution.

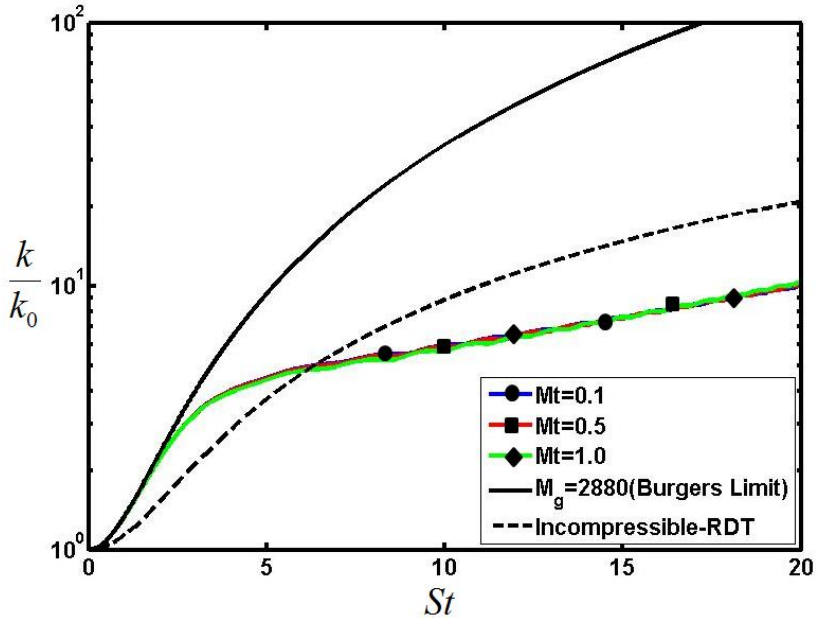

Fig. 36. Evolution of Turbulent Kinetic Energy for various initial turbulent Mach numbers with initial $M_g = 5$ and zero initial temperature fluctuations.

B. Equi-Partition Function

One of the chief findings of Lavin et. al. [11] was that there was equi-partition between the dilatational kinetic energy and the increment in thermal energy. To investigate the influence of initial thermodynamic and velocity fluctuations further we examine the evolution of the equi-partition function:

$$\phi \equiv \frac{\overline{\rho u_2{}^{"} u_2{}^{"}}}{2c_v \rho(\overline{T} - \overline{T}_0)} \tag{5.1}$$

where $\overline{T}_0$ denotes the initial mean temperature. Here $\overline{\rho u_2{}^{"} u_2{}^{"}}$ is the dilatational energy. For a value of $\phi = 1$, there is a perfect equi-partition between the energy modes.

1. Initial Temperature Fluctuation Intensity

In Figure 37 the evolution of the equi-partition function for initial temperature fluctuation cases is presented. Once again, the strong influence of initial temperature fluctuations is evident. Large initial temperature fluctuations cause the partition function to be greater than unity as dilatational fluctuations are generated due to thermal expansion. The larger initial temperature fluctuations, the greater the dilatational energy produced at the initial time. In time, the partition function oscillates about unity indicating a harmonic oscillator type of interaction between thermal and kinetic energies. As time passes the magnitude of the oscillation decreases and equi-partition is achieved.

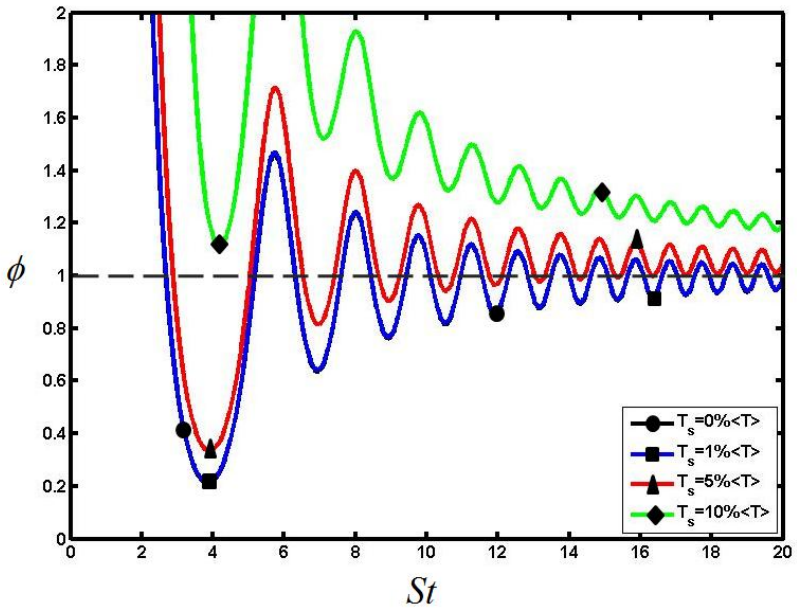

Fig. 37. Evolution of equi-partition for large initial temperature fluctuations with initial $M_g = 5$ and initial $M_t = 0.1$.

2. Initial Turbulent Mach Number

The evolution of the equi-partition function for various initial turbulent Mach numbers is shown in Figure 38. The influence of the turbulent Mach number on the evolution of the equi-partition is nearly negligible.

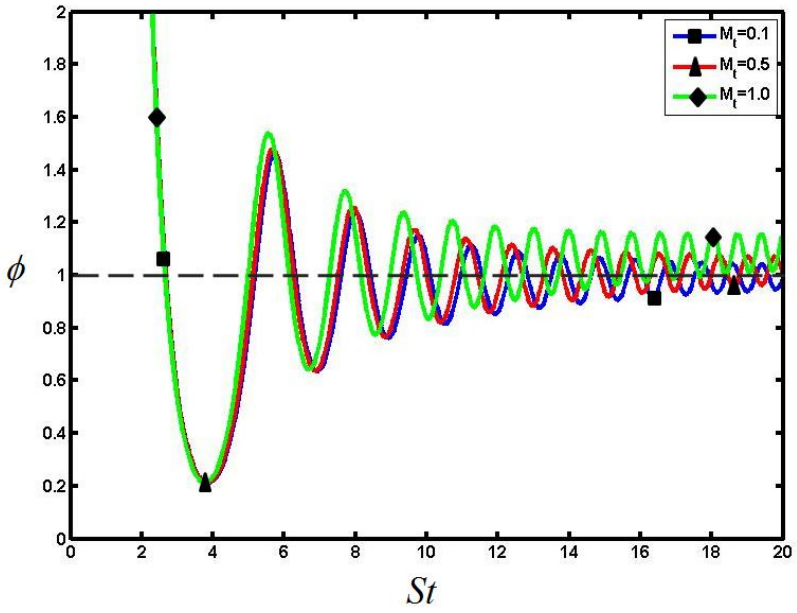

Fig. 38. Evolution of equi-partition function for various initial turbulent Mach numbers with initial $M_g = 5$ and zero initial temperature fluctuations.

C. Influence on Transition Times

Finally, we examine the influence of thermodynamic fluctuations on the three-stage behavior. The two quantities of interest are: (i)Regime 1-2 transition time and (ii) Regime 2-3 transition time.

1. Regime 1-2 Transition Time

This transition time refers to the point in the evolution of turbulent kinetic energy where it peels off of the pressure-released (Burger's turbulence) evolution path. This point is important because it marks the end of the first regime of evolution and the beginning of the second regime. We already stated that the Burger's peel-off time is influenced by the initial gradient Mach number. Now we seek to determine the influence of initial thermodynamic fluctuations on this time. Peel-off times were found for a range of initial conditions.

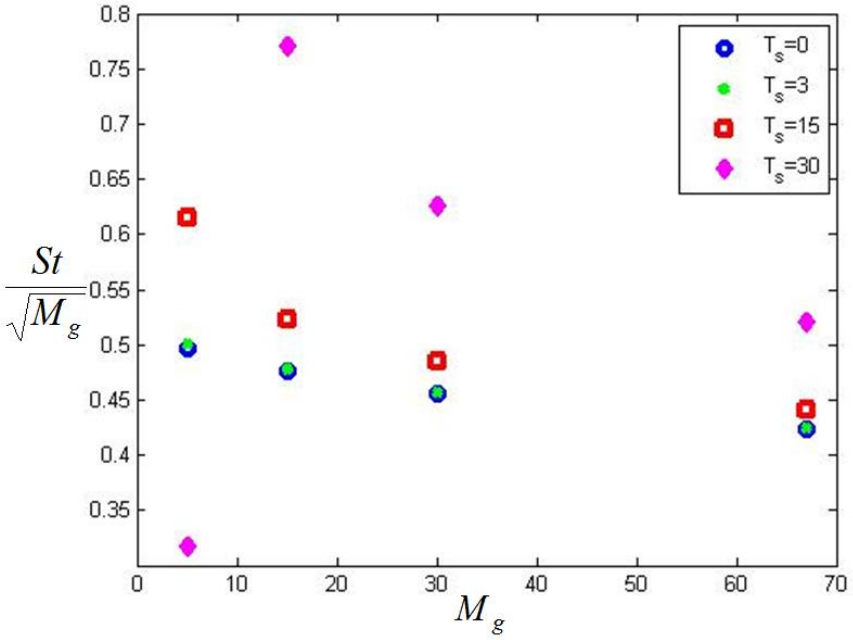

Fig. 39. Regime 1-2 transition times for various initial temperature fluctuations in terms of mixed time.

For a constant initial turbulent Mach number ($M_t = 0.1$) the results are presented in Figure 39. Larger initial temperature fluctuations cause the Burger's peel-off time to occur later, which agrees with Section 1 of this chapter. Even though it is evident that the Burger's peel-off time is dependent on the initial temperature fluctuations,

the exact relationship has yet to be determined.

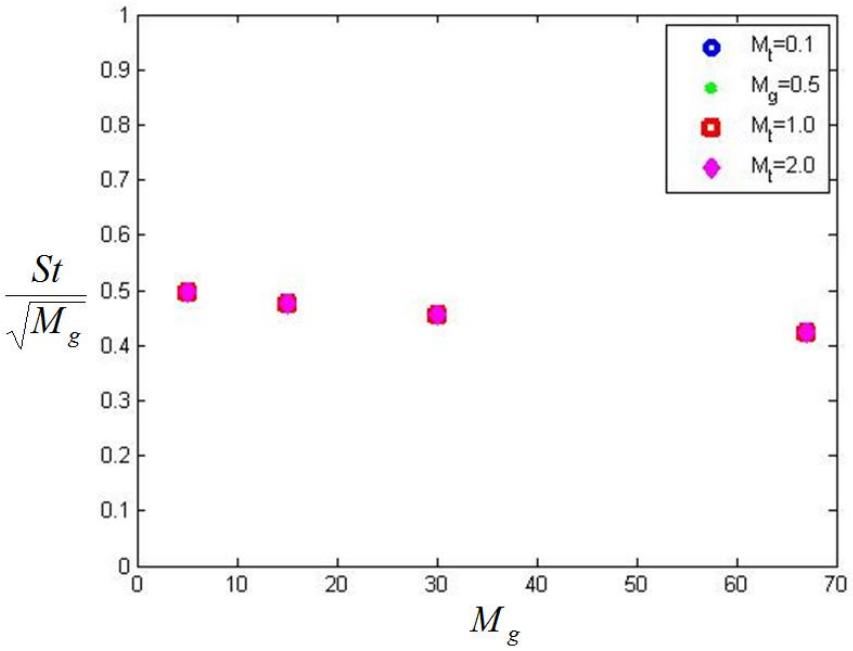

Fig. 40. Regime 1-2 transition times for various M_t values in terms of mixed time.

The results for zero initial temperature fluctuations are presented in Figure 40. This figure is very important in demonstrating the influence of the initial gradient Mach number on Burger's peel-off time. It is clear that transition time is not influenced by the value of the initial turbulent Mach number. Second, the slope of the lines implies a proportional relationship between Burger's peel-off time and the initial gradient Mach number (i.e. $St \approx C * \sqrt{M_g}$).

2. Regime 2-3 Transition Time

This transition time refers to the point where the role of pressure becomes similar to the incompressible flow behavior. We previously suggested that all cases have reached the incompressible regime by one acoustic time. It is important to note

that the transition for each case represents the time when the evolution of each case becomes parallel to the evolution of the incompressible limit case. Therefore, these times occur after the incompressible limit has started.

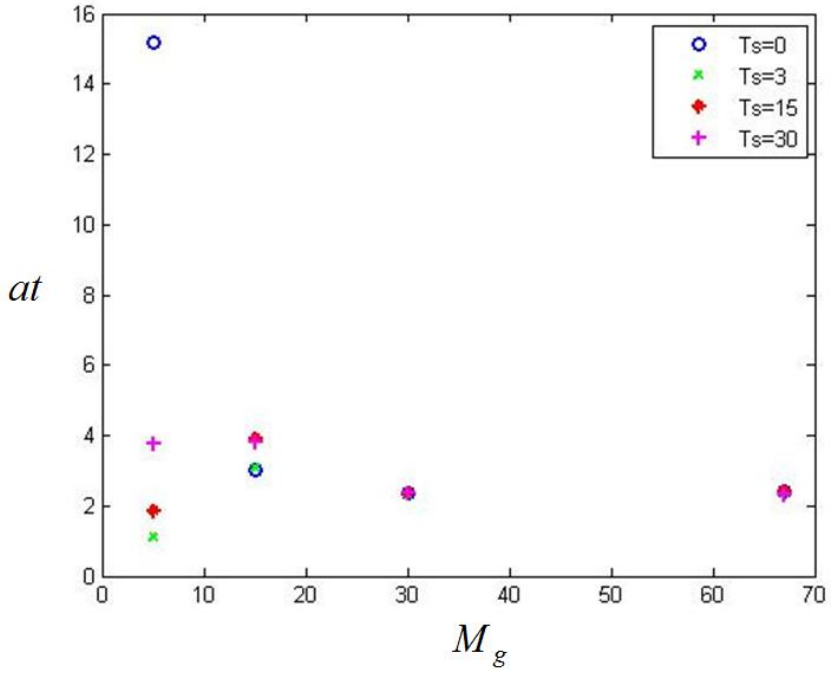

Fig. 41. Regime 2-3 transition times for various initial temperature fluctuations in terms of acoustic time.

For the constant initial turbulent Mach number cases($M_t = 0.1$), the results are displayed in Figure 41. For the smaller initial gradient Mach numbers, a clear relationship between the incompressible limit time and initial temperature fluctuation cannot be found. What is of interest in Figure 41 is how the larger initial gradient Mach number values seem to collapse to a value of 2-3 acoustic times. This discovery supports our claim that regardless of initial conditions, the evolution of the turbulent kinetic energy for compressible RDT will reach the final evolution regime at approximately one acoustic time.

In Figure 42, we present the results of the incompressible limit time for cases of

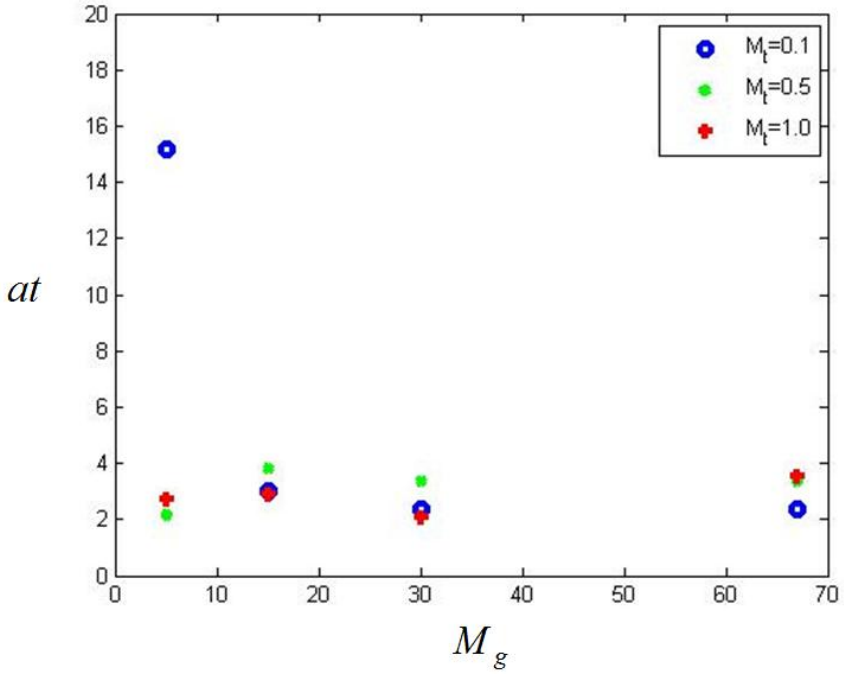

Fig. 42. Regime 2-3 transition times for various initial M_t values in terms of acoustic time.

zero initial temperature fluctuations. Again we see that higher initial gradient Mach numbers support our claim that initial conditions weakly, if at all, influence the onset of the incompressible evolution regime. Another interesting finding in Figure 42 is how the different initial turbulent Mach number cases don't collapse on the same line for larger initial gradient Mach numbers, suggesting that the transition to the final regime may be slightly influenced by the initial turbulent Mach number. For larger gradient Mach numbers, the second transition has occurred by 3-4 acoustic time units.

CHAPTER VI

CONCLUSIONS

The effect of compressibility on shear driven turbulence is of great interest in hypersonic flight applications. It has been known for several years that compressibility has a stabilizing influence and reduces turbulence intensity and mixing. There have been some explanations of the underlying processes using rapid distortion theory (RDT). In this work, a comprehensive demonstration of the stabilizing mechanism is presented. The influence of thermodynamic fluctuations on the stabilizing physics is also investigated.

While previous works have employed Reynolds-averaged RDT, here we also use Favre-averaged RDT. The advantage of F-RDT is a more accurate representation of thermodynamic variables. The most important findings of the work are now summarized.

A. F-RDT Validation

F-RDT results of homogeneous shear compressible turbulence is compared against direct numerical simulation data and R-RDT analysis for intermediate Mach number values. Comparison is made for the kinetic energy growth rate, λ, and b_{12} anisotropy component. F-RDT shows good agreement with the trends of both DNS and R-RDT analysis for the range of initial gradient Mach numbers. The high Mach number ($M_g = 30, 67$) display similar trends throughout, including the oscillatory motion after the maximum peak. F-RDT shows a higher level of accuracy compared to R-RDT when initial velocity fluctuations were introduced. F-RDT achieves values near or at the expected value of the polytropic coefficient (≈ 1.4) for high levels of initial velocity fluctuations whereas the accuracy of R-RDT analysis deteriorates as

the intensity of fluctuations increases.

B. Three timescales

The necessity of investigating evolution in three timescales - shear, acoustic, and mixed - is presented. Each timescale highlights the three-regime evolution of the flow field statistical quantities differently and therefore each timescale has advantages and disadvantages. The main advantage of shear time is the clear transition from regime 1 to regime 2. The precise point of departure from pressure-released turbulence is evident. Shear time also has the disadvantage of only showing two regimes clearly. The acoustic timescale shows all three regimes clearly. It also is beneficial in identifying the expected transition to the third regime ($\approx$ 1 acoustic time). Finally, the geometric mixed time has the advantage of clearly pin-pointing the beginning of the second regime.

C. Three-Regime Evolution

All the statistical quantities of the flow field exhibit a three-regime evolution trend. By examining the evolution of the kinetic energy, the three regions of growth are classified as: (i)rapid growth along the pressure released limit which lasts between 1-2 mixed time units and the gradient Mach number is greater than one, (ii) near-zero growth regime which is complete within one acoustic time when the value of M_g is about unity, and (iii) asyptotic growth similar in trend to the incompressible limit where the gradient Mach number much less than one.

D. Role of Pressure in Three Regimes

The underlying physics in each regime was investigated using the linearized Reynolds-stress evolution equation. The role of the pressure-strain correlation in each regime is as follows: (i) pressure plays a negligent role as production and Reynolds-stress growth rate maintain the same value, (ii)pressure works to nullify the production since the Reynolds-stress growth rate is nearly zero and the magnitude of production is nonzero, (iii) pressure plays a role similar to that of incompressible RDT since the evolution of production and Reynolds-stress growth rate all fall along same path regardless of initial gradient Mach number. Further investigation suggests that pressure evolution in the third regime is governed by Poisson's equation with residual wave effects from the second evolution regime.

E. Effect of Thermodynamic Fluctuations

Analysis of different initial intensities of flow and thermodynamic fluctuations was conducted. Results show the thermodynamic fluctuations have a strong influence on the evolution of the flow field statistics whereas the initial velocity fluctuations only weakly influence the development of the flow field statistics.

F. Transition Times

The final study conducted was to examine the influence of initial flow field fluctuation on the two transition times of the three-regime evolution: (i) Regime 1-2 transition and (ii)Regime 2-3 transition. Initial thermodynamic fluctuations have the affect of delaying the onset of the second regime so Regime 1-2 transition occured later for larger fluctuations. Initial velocity fluctuations showed no effect on Regime 1-2 transition as all cases fell on the same path regardless of initial turbulent Mach

number. Regime 2-3 transition presented no clear qualitative influence from initial flow field fluctuations for smaller gradient Mach numbers. However, larger initial gradient Mach numbers delayed the second transition time to 3-4 acoustic time units.

REFERENCES

[1] S. B. Pope, *Turbulent Flows*. New York, NY: Cambridge University Press, 2000.

[2] G. K. Batchelor and I. Proudman, "The effect of rapid distortion of a fluid in turbulent motion," *Q. J. Mech. Appl. Math.*,vol. 7, no. 1, pp.121-152, 1954.

[3] C. Cambon, G. N. Coleman and D. N. N. Mansour, "Rapid distortion analysis and direct simulation of compressible homogeneous turbulence at finite Mach number," *J. Fluid Mech.*, vol. 257, pp. 641-665, 1993.

[4] G. Brethouwer, "The effect of rotation on rapidly sheared homogeneous turbulence and passive scalar transport, linear theory and direct numerical simulations," *J. Fluid Mech.*, vol. 542, pp. 305-342, 2005.

[5] P.A. Durbin and O. Zeman, "Rapid distortion theory for homogeneous compressed turbulence with application to modeling," *J. Fluid Mech.*, vol. 242, pp. 349-370, 1992.

[6] G. A. Blaisdell, G. N. Coleman and N. N. Mansour, "Rapid distortion theory for compressible homogeneous turbulence under isotropic mean strain," *Phys. Fluids*, vol. 8, pp. 2692-2705, 1996.

[7] G. N. Coleman and N. N. Mansour, "Simulation and modeling of homogeneous compressible turbulence under isotropic mean compression," in *Symposium on Turbulent Shear Flows*. 8th, Munich, Federal Republic of Germany; 9-11 Sept., 1991. pp. 21-3-1 to 21-3-6, 1991.

[8] L. Jacquin, C. Cambon and E. Blin, "Turbulence amplification by a shock wave and rapid distortion theory," *Phys. Fluids A*, vol. 5, no. 10, pp. 2539-2550, 1993.

[9] A. Simone, G. N. Coleman and C. Cambon, "The effect of compressibility on turbulent shear flow: A rapid distortion theory and direct numerical simulation study," *J. Fluid Mech.*, vol. 330, pp. 307-338, 1997.

[10] H. Yu and S. S. Girimaji, "Extension of compressible ideal-gas RDT to general mean velocity gradients." *Phys. Fluids*, vol. 19, no.4, pp. 041702, 2007.

[11] S. Suman, S. S. Girimaji, H. Yu and T. Lavin, "Rapid distortion of Favre-averaged Navier-Stokes equations." Submitted for publication to *J. Fluid Mech.*, in 2010.

[12] S. Suman, S. S. Girimaji and R. L. Bertsch, "Homogeneously-sheared compressible turbulence at rapid distortion limit: Interaction between velocity and thermodynamic fluctuations." *Turbulence, Heat and Mass Transfer 6*, K. Hanjalic, Y. Nagano,and S. Jakirlic Eds. New York: Begell House Inc., pp. 583-586, 2009.

[13] T. Lavin, *Reynolds and Favre-Averaged Rapid Distortion Theory for Compressible, Ideal Gas Turbulence*. M. S. thesis. College Station: Texas A&M University. 2007.

[14] D. Livescu and C. K. Madnia, "Small scale structure of homogeneous turbulent shear flow." *Phys. Fluids*, vol. 16, no. 8, pp. 2864-2876, 2004.

[15] A. M. Savill, "Recent developments in rapid distortion theory." *Ann. Rev. Fluid Mech.* vol. 19, pp. 531-573, 1987.

[16] J. C. R. Hunt and D. J. Carruthers, "Rapid distortion theory and the 'problems' of turbulence." *J. Fluid Mech.*, vol. 212, pp. 497-532, 1990.

[17] S. S. Girimaji, J. R. O'Neil and D. Yu, "Rapid distortion analysis of homogeneous turbulence subjected to rotating shear." *Phys. Fluids*, vol. 18, no. 8, art. no.

085102, 2006.

[18] G. N. Coleman and N. N. Mansour, "Modeling the rapid spherical compression of isotropic turbulence." *Phys. Fluids A*, vol. 3, pp. 2255-2259, 1991.

[19] S. C. Kassinos and W. C. Reynolds, "A particle representation model for the deformation of homogeneous turbulence." *Annual Research Briefs*, Center for Turbulence Research, NASA Ames/Stanford University, pp. 31-53, 1996.

[20] S. S. Girimaji, E. Jeong and S. V. Poroseva, "Pressure-strain correlation in homogeneous anisotropic turbulence subject to rapid strain-dominated distortion." *Phys. Fluids*, vol. 15, no. 10, pp. 3209-3222, 2003.

[21] S. Sarkar, "The stabilizing effect of compressibility in turbulent shear flow." *J. Fluid Mech.*, vol. 282, pp. 163-186, 1995.

VITA

Rebecca Lynne Bertsch was born in Minneapolis, MN, USA. She received her B.A. in physics from Colorado College in May 2007. She began her graduate studies in aerospace engineering at Texas A&M University in August 2007 and graduated with her M.S. in August 2010. She plans to pursue her doctoral degree at Texas A&M University, focusing on the area of compressible turbulence modeling. She can be contacted through Dr. Girimaji at Texas A&M University, Department of Aerospace, H.R. Bright Building, Rm. 701, Ross Street - TAMU 3141, College Station TX 77843-3141.

The typist for this thesis was Rebecca Bertsch.